ORTEC®

AN42
Application Note

Principles and Applications of Timing Spectroscopy

INTRODUCTION

A nuclear detection system consists of one or more detectors that sense the occurrence of nuclear events and of an assortment of instruments that provide information about the events, such as the energy of each event and the time of its occurrence. The term nuclear radiation applies to atomic particles, subatomic particles, gamma rays, and X-rays.

This Application Note is concerned primarily with techniques for measuring the time of occurrence of a nuclear event. Much of the instrumentation that is applicable for time measurements are also common to the instrumentation used for energy measurements.

DETECTION METHODS

Methods for detecting nuclear radiation are usually based on either the excitation of atoms or the liberation of charge in the detecting medium caused by absorption of all or part of the energy of the incident radiation. An example of a device that operates on the principle of excitation of atoms is a scintillation detector. The basic process of detection in the scintillator involves the emission of light from atoms that are excited by the absorption of energy from radiation that passes into the detector. This emitted light is collected by a photomultiplier tube (PMT) and converted into a stream of electrons. Under proper conditions the charge in the current pulse from the PMT is proportional to the energy absorbed in the scintillator.

The principle of charge liberation is the basis on which a semiconductor detector operates. Charges (electron-hole pairs) are liberated in an electric field by the passage of radiation into the detector. A current pulse is produced as the charge is collected on the detector electrodes. Under proper conditions the total charge in the current pulse is proportional to the energy absorbed in the detector from the incident radiation.

ENERGY SPECTROSCOPY

For energy analysis the output current pulse from a PMT or from a semiconductor detector is often applied to a charge-sensitive preamplifier. The preamplifier produces a voltage pulse with a peak amplitude that is proportional to the total charge in the current pulse, which is proportional to the energy absorbed from the incident radiation. Amplifiers and filters are used to expand the range of the peak amplitude and to shape the signal from the preamplifier, a process that maximizes the signal-to-noise ratio for the system. For energy analysis the peak amplitude of the shaped pulse represents the information of interest.

Discriminators and single-channel analyzers (SCA) can be used, following the signal shaping system, to determine the presence of certain energies of detected radiation. A discriminator produces an output logic pulse if it's input signal exceeds a preset threshold level. An SCA produces an output logic pulse if the peak amplitude of it's input signal falls within the energy window that is established with two preset threshold levels.

A multichannel analyzer (MCA) operates like a parallel array of single-channel analyzers that have been adjusted to have adjacent window segments within a range of energies. The MCA separates the output signals that are furnished from the signal shaping system into incremental ranges of pulse heights and accumulates the number of pulse measurements falling within each range. These increments correspond to ranges of energies in the detected radiation. The stored information can be used to provide a histogram representing the probability density of pulse heights, or energies, of the detected radiation. The MCA also provides means for the stored data to be displayed, printed, or plotted, or to be used by a computer for further analysis.

TIME SPECTROSCOPY

Time spectroscopy involves the measurement of the time relationship between two events. A particularly difficult problem in timing is to obtain a signal that is precisely related in time to the event. A time pick-off circuit is employed to produce a logic output pulse that is consistently related in time to the beginning of each input signal. Ideally, the time of occurrence of the logic pulse from the time pick-off element is insensitive to the shape and amplitude of the input signals.

A time-to-amplitude converter (TAC) can be used to measure the time relationship between correlated or coincident events seen by two different detectors that are irradiated by the same source. Figure 1 is a simplified block diagram of a typical time spectrometer used for making this type of timing measurement. A time pick-off unit is associated with each detector, with the

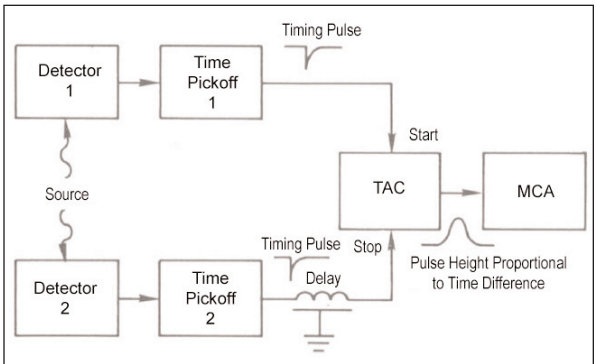

Fig. 1. Simplified Block Diagram of a Typical Time Spectrometer.

logic pulse from one time pick-off used to start the TAC and the delayed logic pulse from the other time pick-off used to stop the TAC. The TAC is usually implemented by charging a capacitor with a constant-current source during the time interval between a start input signal and the next stop input signal. The amplitude of the voltage on the capacitor at the end of the charging interval is proportional to the time difference between the two signals. The delay shown in Figure 1 separates the start and stop signals sufficiently to permit the TAC to operate in it's most linear region.

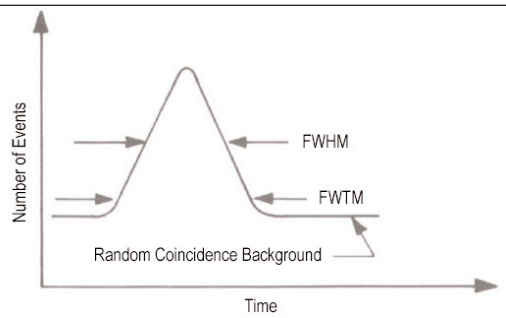

Fig. 2. Timing Coincidence Spectrum.

The amplitude information from the TAC is often applied to an MCA for accumulation of the data and display of the probability density of the start-to-stop time intervals, commonly called a timing spectrum. Figure 2 indicates a type of timing spectrum that might be produced by coincident gamma rays. The shape of the timing spectrum is critically important in time spectroscopy. The timing resolution must be high (the timing peak must be narrow) so that the time relationship between two closely spaced events can be measured accurately. It is important that the narrow width of the spectral peak be maintained down to a small fraction of it's maximum height to ensure that all truly coincident events are recorded. One figure of merit is the full width of the timing peak at one-tenth it's maximum value (FWTM). For a Gaussian time distribution the total number of counts included in this measurement represents about 98% of the true coincident events. Another figure of merit is the full width of the timing peak at one-half its maximum value (FWHM). The integral number of counts included in this measurement, for a Gaussian timing distribution, represents about 76% of the total number of coincident events. At some point the sides of the timing peak merge into the random coincidence background.

In some timing applications it is sufficient to know that two detected events were coincident within the limits of a short time interval. This type of measurement, as opposed to the multichannel method shown in Fig.1, may be considered as a single-channel of time-window analysis. The term window indicates that there is a certain range of time during which, if both input signals are present, a logic pulse is generated to indicate the coincidence. Pairs of input signals that do not occur within this time window, relative to each other, are not recognized. The minimum permissible width of the time window is limited by the time pick-off devices. If the time window is narrower than the width of the timing peak shown in Figure 2, some of the events that are truly coincident will be rejected. Therefore, the width of the time window is usually set slightly wider than the FWTM value of the time spectrum.

There are two general techniques for processing pulses in an overlap type of coincidence recognition instrument: the slow-coincidence method and the fast-coincidence method. The slow-coincidence method uses the width of the input pulses directly in a time overlap evaluation. The fast-coincidence method provides an internally reshaped pulse so that there is a standardized pulse width for each input signal and then detects any overlap of the standardized pulses. An advantage of using the fast-coincidence method is that adjusting the width of the reshaped pulses can control the resolving time, or time window.

Figure 3 shows a simplified fast-coincidence system that uses single-channel or time-window analysis. The input pulses to the coincidence module are reshaped to a standard width, τ. If the reshaped pulses have a time overlap, a logic pulse is produced at the output. The resolving time or time-window width of the fast-coincidence unit must be carefully adjusted to ensure that genuinely coincident events produce and output pulse. In addition, this system produces only a logic decision concerning the coincidence, neither resolving the actual time difference between two input signals nor indicating which of the two signals occurred first.

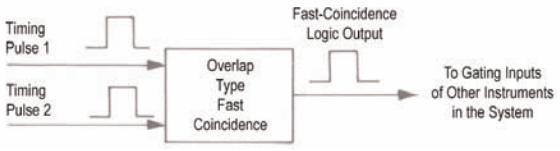

Fig. 3. Single-Channel Fast-Coincidence System Using an Overlap Type of Coincidence Circuit.

The coincidence system shown in Figure 4 overcomes some of the disadvantages of the overlap type of system and also provides timing resolution information. In this system an SCA is used to select the range of pulse amplitudes from the TAC that represents true-coincidence events. The SCA window (i.e., the region of interest in the timing spectrum) can be set quickly and accurately while the timing information from the TAC is accumulated in a multichannel analyzer. The TAC output is used to generate a spectrum for the display by the MCA, which is gated by the SCA output. The output of the SCA can also be used to gate other instruments in the system.

A second SCA may be used to monitor the random coincidence background, which in Figure 4, is the area of the spectrum not included in the time window. The second SCA window width is set equal to the first but it is positioned in the flat random coincidence background portion of the spectrum. Ideally the number of random coincidence events selected by the second SCA is then identical to the number that is detected by the first SCA. By recording a gated timing spectrum for each SCA, the true-coincidence spectrum can be corrected by a channel-by-channel subtraction procedure.

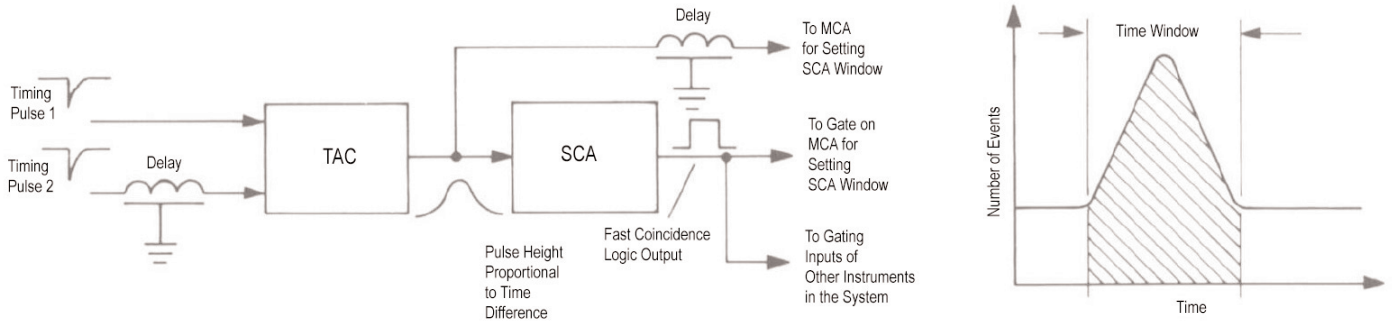

Fig. 4. Single-Channel Fast-Coincidence System Using a Time-to-Amplitude converter, TAC, and the MCA Display to Set the Time Window.

TIME PICK-OFF TECHNIQUES

A time pick-off element is essential in all timing systems. An ideal time pick-off produces a logic pulse at it's output that is precisely related in time to the occurrence of an event. Three important sources of error can occur in time pick-off measurements: walk (sometimes called time slewing), drift, and jitter.

Walk is the time movement of the output pulse from the pick-off element, relative to it's input pulse, due to variations in the shape and amplitude of the input pulse. Drift is the long-term timing error introduced by component aging and by temperature variations in the time pick-off circuitry. Jitter is the timing uncertainty of the pick-off signal that is caused by noise in the system and by statistical fluctuations of the signals from the detector. Timing jitter is usually dominated by the statistical behavior of the signals from the detector system rather than by electronic noise.

In scintillator/photomultiplier timing systems, the sources of jitter are:

1) the variation of the generation rate of photons in the scintillator

2) the transit time variation of photons through the scintillator

3) the transit time variation of the photoelectrons in the PMT

4) the gain variation of the PMT

Jitter sources 1) and 4) can contribute to the pulse-height variations of the PMT output signals. Sources 1), 2), and 3) affect the time of occurrence of the PMT output signals and to some extent their shape.

In semiconductor detector systems and more specifically in germanium coaxial detectors, timing properties are determined primarily by time slewing (walk) resulting from the shape of the detector output pulse. The detector pulse shape is dependent on the charge transit time which is influenced by the electric field as a function of position in the detector, by electron and hole mobilities, and by the distribution of the charge created by the detected radiation. These three important sources of error are discussed in greater depth as they apply to the following principal types of time pick-off technique. Other sources of variations in charge collection time are charge trapping, which is due to crystal defects or impurities, and the plasma effect.

LEADING EDGE

A leading-edge discriminator is the simplest means of deriving a time pick-off signal and produces an output logic pulse when the input signal crosses a fixed threshold level. A primary disadvantage of this technique is that the time of occurrence of the output pulse from a leading-edge trigger is a function of the amplitude and rise time of the input signal. This time slewing relationship restricts the usefulness of the leading-edge trigger as an accurate time pick-off device to those applications that involve only a very narrow range of input signal amplitudes and rise times.

Figure 5 illustrates the time walk of an ideal leading-edge discriminator caused by variations in the amplitude and rise time of it's input signals. Signals A and B are input pulses that have the same rise time but different amplitudes. Although these

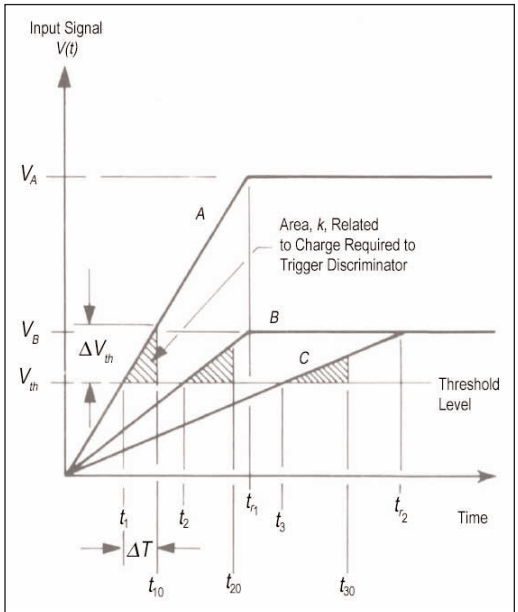

Fig. 5. Walk in a Leading-Edge Discriminator Due to Amplitude and Rise Time Variations and Charge Sensitivity.

signals occur simultaneously, they cross the threshold level, V_{th}, at different times, t_1 and t_2. Signals B and C are input pulses that have the same amplitude but different rise times and they occur simultaneously but cross the threshold level at different times, t_2 and t_3. These differences in threshold-crossing time cause the output logic pulse from the discriminator to "walk" along the time axis as a function of the input signal amplitude and rise time. The walk is most pronounced for signals with amplitudes that only slightly exceed the threshold level. Walk is significantly reduced for signals with shorter rise times and for signals that greatly exceed the threshold level of the leading-edge discriminator.

An additional contribution to the time walk of a real leading-edge discriminator is it's charge sensitivity, a term that describes the small amount of charge that is required to trigger a physically realizable threshold or crossover detecting device. Time walk due to charge sensitivity is also illustrated in Figure 5. After an input signal crosses the discriminator threshold level, a small additional amount of charge is required to actually trigger the discriminating element. The time required to accumulate this additional charge is related to the areas of the shaded triangles by the impedance of the discriminator. Thus times t_{10}, t_{20}, and t_{30} are the times at which the output signals actually occur, relative to times t_1, t_2, and t_3, respectively, at which the input signal cross the threshold level. For input signals that have identical amplitudes and the timing error introduced by charge sensitivity is greater for signals with longer rise times. For input signals that have identical rise times the time delay introduced by charge sensitivity is greater for signals with smaller pulse heights. In principle, for a flat top pulse of infinite duration the time required to accumulate the additional charge approaches infinity as the pulse height approaches the discriminator threshold. In practical cases however, the walk due to charge sensitivity is limited by the width of the pulse above the discriminator threshold level.

Charge sensitivity introduces changes in the effective threshold level of a leading-edge discriminator, as well as changes in its effective sensing time. These changes are related to the slope of the input signal as it passes through the threshold. For simplicity it can be assumed that the input signal is approximately linear during the time, Δt, that is required to accumulate the charge-related area, k, indicated in Figure 5. The error in the effective sensing time is related to the slope of the input signal by

$$\Delta T \cong \sqrt{\frac{2k}{\left.\frac{dV(t)}{dt}\right|_{t=T}}} \qquad (1)$$

Where V(t) is the input signal as a function of time and T is the threshold-crossing time of V(t). As can be seen in Figure 5, although signals with shorter rise times tend to decrease the time walk of a leading-edge discriminator due to charge sensitivity, they increase the error in its effective threshold level.

As was mentioned earlier, jitter, another major source of error in time pick-off techniques, refers to the timing uncertainty caused by statistical fluctuations of the signals from the detector and by noise. The noise can be present on the detector signal, can be generated the processing electronics, or can be generated by the discriminator itself. Statistical amplitude fluctuations of the detector signals and noise on the input signal to a leading-edge discriminator cause and uncertainty in the time at which the signal crosses the discriminator threshold level. These two sources of timing uncertainty are illustrated in Figure 6 for an ideal leading-edge discriminator.

Assuming a Gaussian-probability density of noise amplitude with zero mean, let the standard deviation (or rms value) of the noise be σ_V. The noise-induce rms uncertainty, σ_T, in threshold-crossing time for the leading-edge discriminator is given with reasonable accuracy by the triangular rule as

$$\sigma_T \cong \frac{\sigma_V}{\left.\frac{dV(t)}{dt}\right|_{t=T}} \qquad (2)$$

In obtaining this expression the input signal, V(t), is assumed to be approximately linear in the region of threshold crossing, and the discriminator threshold level is assumed to be removed from both zero

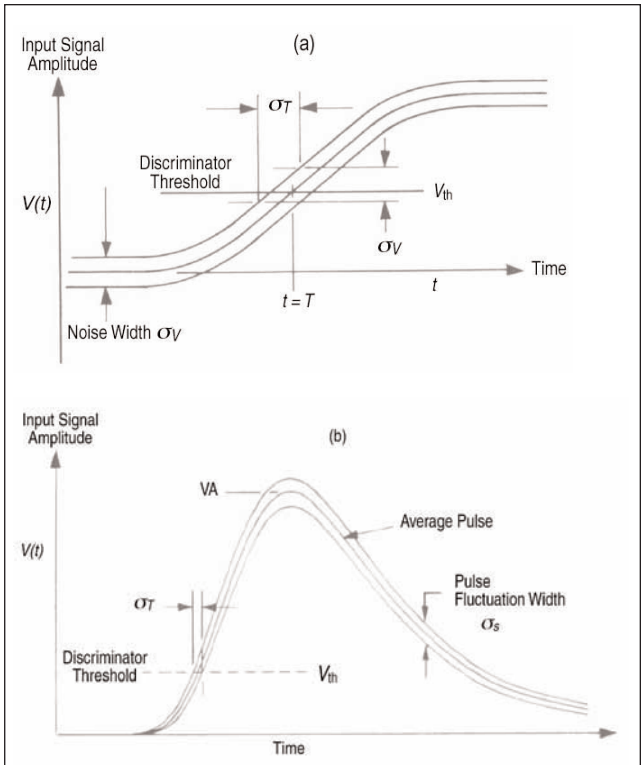

Fig. 6. Time Jitter in a Leading-Edge Discriminator Due to (a) Noise on the Input Signal and (b) Statistical Pulse-Height Variations.

level and the peak amplitude of the signal by at least the noise width. The timing uncertainty cause by statistical amplitude fluctuations of the detector signal can be approximated in a similar manner for leading-edge timing.

If several sources of statistical timing uncertainty can be identified, the rms jitter due to each source can be determined. The total rms time jitter can be approximated by the square root of the sum of the squares of the individual rms jitter components. Timing uncertainty due to noise and statistical amplitude variations of the detector signals is directly related to the amplitude of the fluctuations of the input signal. The timing uncertainty due to these sources of jitter is inversely proportional to the slope of the input signal at threshold-crossing time. In general, signals with greater slopes at threshold crossing produce less time jitter.

When the leading-edge technique is restricted to those applications that involve a very narrow dynamic range of signals, excellent timing results can be obtained. Under these conditions timing errors due to charge sensitivity and jitter are minimized for input signals with the greatest slope at threshold-crossing time. The best timing resolution is most frequently found by experimenting with the threshold level.

CONSTANT FRACTION

The existence of an optimum triggering fraction for leading-edge timing with plastic scintillator/photomultiplier systems stimulated the design for a circuit that would trigger at the optimum triggering fraction regardless of the pulse height. Based on leading-edge timing data, the optimum fractional point on the leading edge of the amplifier output pulse was selected as the one at which the best time resolution could be obtained.

A functional representation of a constant-fraction trigger is shown in Fig. 7. In the constant-fraction method the input signal to the circuit is delayed, and a fraction of the undelayed pulse is subtracted from it. A bipolar pulse is generated and it's zero crossing is detected and used to produce an output logic pulse. The use of a leading-edge arming discriminator provides energy selection capability and prevents the sensitive zero-crossing device from triggering on the noise on the constant-fraction baseline. A one-shot multivibrator is used to prevent multiple output signals form being generated in response to a single input pulse.

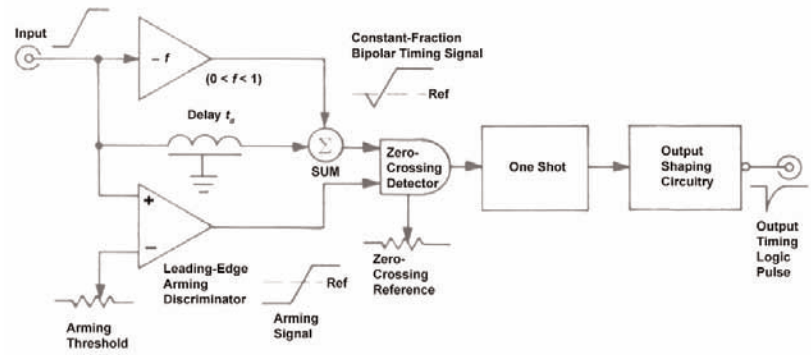

Fig. 7. Functional Representation of a Constant-Fraction Trigger.

With the constant-fraction technique, walk due to rise time and amplitude variations of the input signals is minimized by proper selections of the shaping delay time, t_d. Jitter is also minimized for each detector by proper selection of the attenuation fraction, f, that determines the triggering fraction. Although difficult to implement, the constant-fraction trigger can provide excellent timing results over a wide dynamic range of input signals.

Two cases must be considered in determining the zero-crossing time for the constant-fraction bipolar signal. The first case is for true-constant-fraction (TCF) timing, and the second is for the amplitude-and-rise-time-compensated (ARC) timing.

In the true-constant-fraction case the time of zero crossing occurs while the attenuated input signal is at its full amplitude. This condition allows the time pick-off signal to be generated at the same fraction, f, of the input pulse height regardless of the amplitude. Figure 8 illustrates the signal formation in an ideal constant-fraction discriminator for TCF-timing with linear input signals. The amplitude independence of the zero-crossing time is depicted for input signals A and B, which have the same rise time, t_{r1}, but different amplitudes. From signals B and C the zero-crossing time for TCF case is seen to be dependent on the rise time of the input signals. For linear input signals that begin at time zero the constant-fraction zero-crossing time, T_{TCF}, for the true-constant-fraction case is

$$T_{TCF} = T_d + ft_1 \qquad (3)$$

Two criteria for the constant-fraction shaping delay, t_d, must be observed in order to ensure TCF timing for each linear input signal. The shaping delay, t_d, must be selected so that

$$t_d > t_r\,(1 - f) \qquad (4)$$

This constraint ensures that the zero-crossing time occurs after the attenuated linear input signal has reached it's maximum amplitude. Practical timing experiments involve input signals with finite pulse widths; therefore the shaping delay, t_d, must also be made short enough to force the zero crossing of the constant-fraction signal to occur during the time that the attenuated signal is at

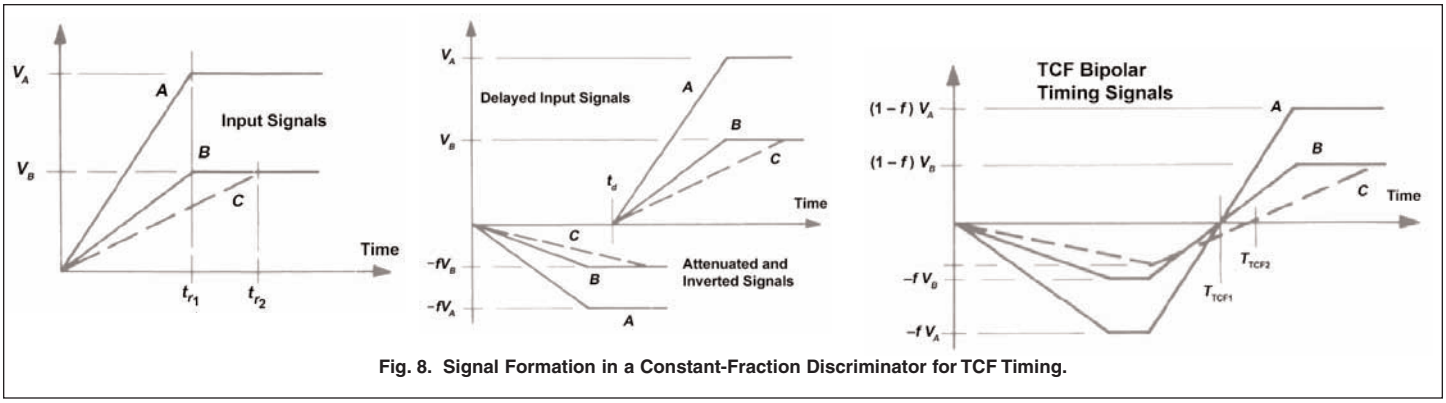

Fig. 8. Signal Formation in a Constant-Fraction Discriminator for TCF Timing.

it's peak. Observing these two criteria allows the time pick-off signal to be generated at the fraction, f, of the input pulse height regardless of the amplitude.

From Equation (3) and the criteria for t_d, true-constant-fraction timing is seen to have limitations in it's application. TCF timing is most effective when used with input signals having a wide range of amplitudes but having a narrow range of rise times and pulse widths. These input signal restrictions favor the use of TCF timing in scintillator/photomultiplier systems. Any remaining walk effect can be attributed to the charge sensitivity of the zero-crossing detector and the slew limitations of the devices used to form the constant-fraction signal.

The second case to be considered in determining the zero-crossing time of the constant-fraction signal is for ARC timing, when the time of zero crossover occurs before the attenuated input signal has reached it's maximum pulse height. This condition eliminates the rise-time dependence of the zero-crossing time that limits the application of the TCF technique. Figure 9 illustrates the signal formation in an ideal constant-fraction discriminator for ARC timing with linear input signals. The amplitude independence of the ARC zero-crossing times is depicted for input signals B and C, which have the same amplitude, V_B, but different rise times. For linear input signals that begin at time zero the zero-crossing time, T_{ARC}, for the ARC timing case is

$$T_{ARC} = \frac{t_d}{1 - f} \qquad (5)$$

One of the criteria for td that must be observed in order to ensure ARC timing with linear input signals is

$$t_d < t_{r(min)} (1 - f) \qquad (6)$$

where $t_{r(min)}$ is the minimum expected rise time for any input signal. This constraint ensures ARC timing for all linear input signals with rise times greater than $t_{r(min)}$, regardless of the input pulse width.

In ARC timing the fraction of the input pulse height at which the time pick-off signal is generated is not constant. The effective triggering fraction for each input pulse is related to the attenuation fraction, f, by the input signal rise time. Thus for linear input signals the effective ARC-timing triggering fraction is

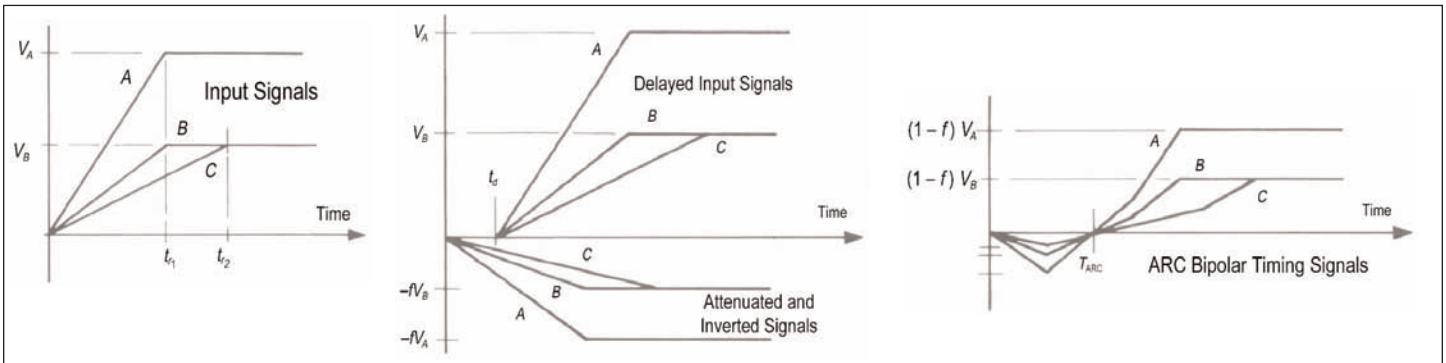

Fig. 9. Signal Formation in a Constant-Fraction Discriminator for ARC Timing.

$$f_{ARC(eff)} = \frac{ft_d}{t_r(1-f)} \qquad (7)$$

which is always less than f.

ARC timing is most useful when the input signals have a wide range of amplitudes and rise times making it especially suitable for use with large-volume germanium detectors that have wide variations in charge collection times. Jitter is a limiting factor in ARC timing with a narrow dynamic range of input signals.

As was mentioned previously, the constant-fraction trigger was originally developed to provide a time pick-off signal at the fraction of input pulse amplitude at which timing error due to jitter is minimized. Noise-induced time jitter for an ideal constant-fraction trigger is illustrated in Figure 10 for TCF timing with linear input signals.

The noise-induced rms uncertainty in the constant-fraction zero-crossing time, $\sigma_{T(cf)}$, is given

$$\sigma_{T(cf)} \cong \frac{\sigma_{V(cf)}}{\left.\frac{dV_{cf}(t)}{dt}\right|_{t = T_{cf}}} \qquad (8)$$

where

$\sigma_{V(cf)}$ is the standard deviation (or rms value) of the noise on the constant-fraction bipoar signal, $V_{cf}(t)$,

T_{cf} is the general zero-crossing time for either TCF or ARC timing.

In Equation (8) the constant-fraction composite signal, $V_{cf}(t)$, is assumed to be approximately linear in the region of zero crossing, and the rms value of it's noise can be related to the noise on the input signal. The following additional assumptions are also made to simplify this relationship: the noise on the input signal is a time-stationary random process, having a Gaussian-probability density function of amplitudes with a zero mean value; and the constant-fraction circuit is ideal, having an infinite bandwidth and contributing zero noise. Then

$$\sigma_{V(cf)} = \sigma V \sqrt{1 + f^2 - \frac{2f\Phi(t_d)}{\overline{V_n^2(t)}}} \qquad (9)$$

where

σ_V is the rms value of the input noise,

f is the constant-fraction attenuation factor,

$V_n^2(t)$ is the mean-squared value of the input noise,

$\Phi(t_d)$ is the autocorrelation function of the input noise,

t_d is the constant-fraction shaping delay.

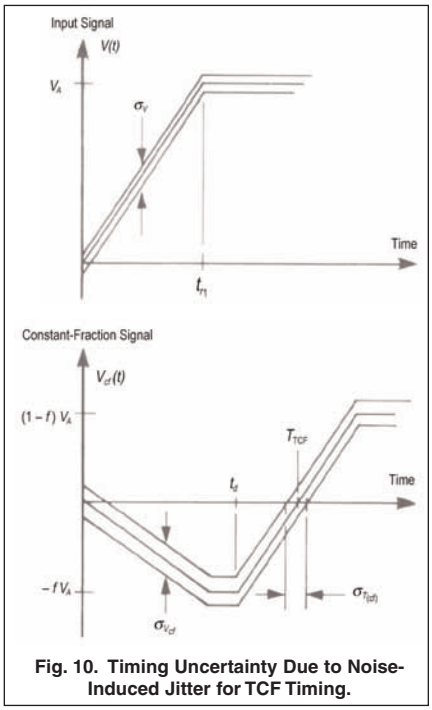

Fig. 10. Timing Uncertainty Due to Noise-Induced Jitter for TCF Timing.

For cases of uncorrelated noise the rms value of the noise on the constant-fraction signal is related to the rms value of the noise on the input signal by

$$\sigma_{V(cf)} = \sigma_V \sqrt{1 + f^2} \qquad (10)$$

Equation (10) is quite useful in estimating the timing error due to noise-induced jitter given by Equation (8).

Determining the constant-fraction time jitter due to noise from Equation (8) also requires knowledge of the slope of the composite timing signal at the crossover. For TCF timing with a linear input signal the slope of the bipolar timing signal at crossover is

$$\left.\frac{dV_{cf}(t)}{dt}\right|_{t = T_{TCF}} = \frac{V_A}{t_{r1}} \qquad (11)$$

For ARC timing with a linear input signal the slope of the constant-fraction signal at zero crossing is

$$\left.\frac{dV_{cf}(t)}{dt}\right|_{t = T_{ARC}} = \frac{(1 - f)\, V_A}{t_{r1}} \qquad (12)$$

Combining equations (10) and either (11) or (12) with equation (8) yields the following expressions for noise-induced time jitter with linear input signals:

For TCF timing

$$\sigma_{T(TCF)} \cong \frac{\sigma_V \sqrt{1 + f^2}}{V_A / t_{r1}} \qquad (13)$$

For ARC timing

$$\sigma_{T(ARC)} \cong \frac{\sigma_V \sqrt{1 + f^2}}{V_A\,(1 - f)/t_{r1}} \qquad (14)$$

A study of Equation (2) and Equations (8) through (14) lead to several interesting observations concerning noise-induced jitter for constant-fraction timing and for leading-edge timing. For example, for the uncorrelated-noise case, which is the simplest and most prevalent case, under identical input signal and noise conditions and for the same attenuation fraction, f, the timing error due to noise-induced jitter is usually worse for ARC timing than it is for TCF timing. Although the rms value of the noise on the bipolar timing signal at zero crossing is the same in both cases, the slope of the ARC timing signal at zeros crossing is almost always less than the slope of the TCF signal at zero crossing.

Under the conditions of identical input signal, noise, and fractional triggering level, the timing error due to noise-induced jitter should be worse for TCF timing than for leading-edge timing. The rms value of the noise is greater on the TCF bipolar signal than on the input signal by a factor of approximately $\sqrt{1 + f^2}$. Ideally, the slopes of the two timing signals would be the same at the pick-off time. However, TCF timing virtually eliminates time jitter due to statistical amplitude variations of the signals from the detector. Thus if statistical amplitude variations are more predominant than noise, the timing uncertainty due to jitter with TCF timing can be less than that with leading-edge timing.

Time walk due to the charge sensitivity of the zero-crossing detector should also be considered. Equation (1) indicates that the delay time due to charge sensitivity is inversely proportional to the square root of the slope of the timing signal at the threshold-crossing (or zero-crossing) time. The timing signal is assumed to be approximately linear in the crossover region. Thus for identical input signals and for the same attenuation faction, f, the time delay (or walk time) due to charge sensitivity is usually greater for ARC timing than for TCF timing. The slope of the ARC timing signal at zero crossing is almost always less than the slope of the TCF bipolar signal at zero crossing.

Although the constant-fraction technique is more difficult to implement than the leading-edge technique, it provides excellent timing results in a variety of applications. True-constant-fraction timing is most effective when used with input signals having a wide range of amplitudes but a narrow range of rise times and pulse widths. Amplitude and rise-time compensated timing is most effective when used with input signals having a wide range of amplitudes and rise times regardless of pulse width. For a very narrow dynamic range of input signal amplitudes and rise times, leading-edge timing may provide better timing resolution if the timing jitter is dominated by noise rather than be statistical amplitude variations of the detector signals.

In practice, an additional problem is encountered with the ARC timing technique: the constant-fraction discriminator can produce leading-edge time walk. A leading-edge discriminator is commonly used to arm the zero-crossing detector in a constant-fraction discriminator. To provide ARC timing the zero-crossing detector must be armed during the time interval between the initiation of the constant-fraction signal and it's zero crossing. If the sensitive crossover-detection device is armed before the bipolar timing pulse begins, the pick-off signal is generated by random noise on the constant-fraction baseline. If the leading edge occurs after zero crossing time, the unit produces leading edge timing. This type of timing error occurs most often in ARC timing for signals with exceptionally long rise times and for signals with peak amplitudes that exceed the threshold level by only a small amount.

Several techniques have been devised to eliminate leading-edge walk effects in ARC discriminators. A slow-rise-time (SRT) reject circuit can be used to evaluate the relative times of occurrence of the constant-fraction signal and the leading-edge arming signal and then to block the timing logic pulses produced by leading-edge timing. This technique improves timing resolution below the FWHM level at the expense of counting efficiency in the discriminator.

PRACTICAL CONSTANT-FRACTION CIRCUITS

Many different circuits have been used to form the constant-fraction signal. The discussion associated with Figure 7 described the principal functions that must be performed including the attenuation, delay, inversion, summing, arming the zero-crossing detector, and detection of the zero crossing of the constant-fraction bipolar timing signal. Since the input circuit sets many of the ultimate performance characteristics of the constant-fraction discriminator, a brief description of the principal circuits in use may be helpful.

The block diagrams of the input circuits of four ORTEC Constant-Fraction Discriminators are shown in Figure 11. The simplest circuit is shown in Figure 11(a). The upper comparator is a leading-edge discriminator whose output arms the zero–crossing detector. The constant-fraction signal is formed actively in the input differential stage of the lower comparator. The monitor signal is taken at the output of the constant-fraction comparator and is clamped at about 400-millivolts peak-to-peak. The lowest threshold setting for this circuit is approximately 5-millivolts and is determined by the characteristics of the leading-edge comparator.

Figure 11(b) show another input circuit. In this circuit, the constant-fraction signal is formed passively in a differential transformer. The bandwidth of the transformer is very high (>400 MHz). The monitor output is a close approximation of the actual constant-fraction signal since it is picked-off at the input to the constant-fraction comparator. The arming and zero-crossing detector circuits are the same as in Figure 11(a). The minimum threshold is 30-millivolts.

A third input circuit is shown in Figure 11(c). An additional leading-edge comparator has been added. The upper leading-edge comparator sets the energy range while the lower leading-edge comparator performs the arming function. Any input signal that crosses the upper leading-edge comparator threshold is sufficiently large to ensure and overdrive signal to the arming comparator whose threshold is set at E/2. This dual comparator arrangement effectively removes leading-edge walk for a signal just slightly greater than the E threshold level. The minimum value of the E threshold is 50-millivolts. The monitor output is similar to the circuit shown in Figure 11(a) and is limited to about 400-millivolts peak-to-peak. This circuit in Figure 11(c) also has three internal delay cables nominally optimized for use with plastic scintillators, NaI (Tl), and Ge detectors. The appropriate delay is switch-selected on the front panel.

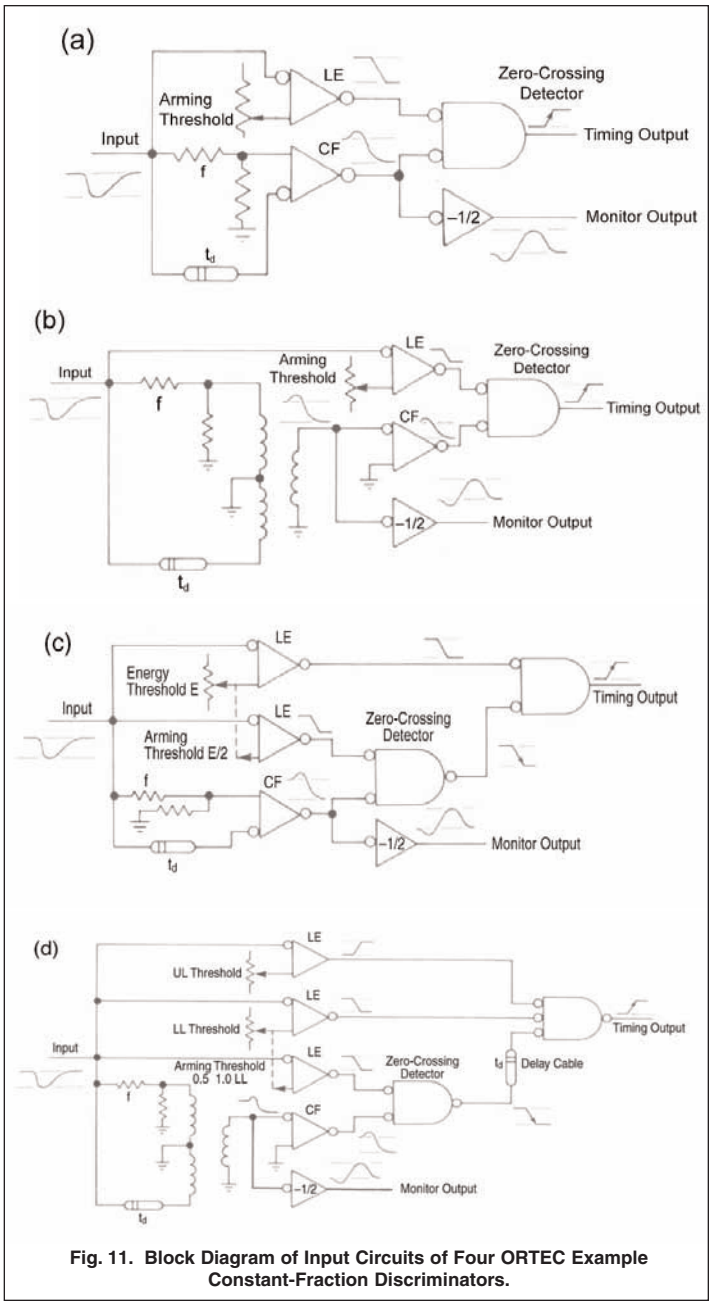

Fig. 11. Block Diagram of Input Circuits of Four ORTEC Example Constant-Fraction Discriminators.

In Figure 11(d) a third leading-edge comparator has been added to allow selection of an upper energy of interest. Thus this circuit is a differential discriminator that can be adjusted to respond to the input signals corresponding to a limited energy range. An output is produced when the input signal exceeds the lower-level threshold and does not exceed the upper-level threshold. This feature is also useful when selecting a single photon level, double photon level, or some other unique input signal condition. Figure 11(d) uses the same differential transformer techniques as those used in Figure 11(b), and it's monitor output is a faithful reproduction of the constant-fraction signal. The arming threshold can be adjusted from 0.5 to 1.0 times the lower-level threshold setting. The minimum threshold is 30-millivolts.

FAST CROSSOVER

The fast-crossover time pick-off technique was developed to overcome the serious walk effects inherent in the use of the leading-edge method with a wide dynamic range of signals. This technique is specifically intended for use with the anode signal from fast scintillator/photomultiplier systems. The anode current pulse from the photomultiplier tube is stub-clipped with a shorted delay line to produce a bipolar timing signal. After the zero crossing off the timing pulse id detected, it is used to produce an output logic pulse. For signals with the same pulse shape but with a wide dynamic range of amplitudes the zero crossing represents the same phase point on all input signals. Most of the amplitude-dependent time walk is eliminated, and what walk remains is due to the charge sensitivity of the zero-crossing detector.

Formation of the bipolar timing signal for the fast-crossover technique is shown in Figure 12. The amplitude independence of the zero-crossing time is depicted for signals for different amplitudes that have identical pulse shapes. When this time pick-off method is used, identical pulse shapes are critical.

The noise-induced rms uncertainty, $\sigma_{T(fz)}$, in the zero-crossing time of the fast-crossover signal is given with reasonable accuracy by the triangle rule as

$$\sigma_{T(fz)} \cong \frac{\sigma_{V(fz)}}{\left.\frac{dV_{fz}}{dt}\right|_{t = T_{fz}}} \qquad (15)$$

where

$\sigma_{T(fz)}$ is the standard deviation (or rms value) of the noise on the bipolar timing signal, $V_{(fz)}(t)$,

T_{fz} is the zero-crossing time.

The composite bipolar signal, $V_{fz}(t)$, is assumed to be approximately linear in the region of zero-crossing.

In Equation (15) the rms value of the noise on the bipolar timing signal is related to the rms value of the noise on the input signal by

$$\sigma_{T(fz)} \cong \sigma_V \sqrt{(1)^2 + (1)^2 - \frac{2\Phi(2t_d)}{V_n^2(t)}} \qquad (16)$$

where

σV is the rms value of the input noise,

$V_n^2(t)$ is the mean-squared function of the input noise,

$\Phi(2t_d)$ is the autocorrelation function of the input noise,

t_d is the delay time of the shored-delay-line stub.

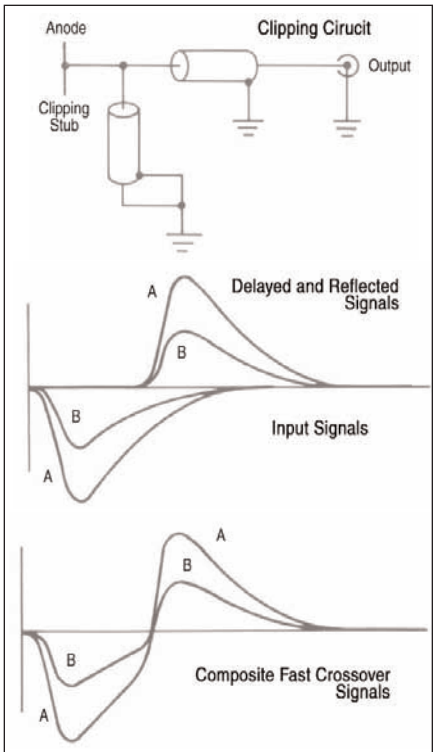

Fig. 12. Stub-Clipping Signal Formation for Fast-Zero Crossover.

The noise on the input signal is assumed to be a time-stationary random process, having a Gaussian-probability density function of amplitudes with a zero mean value. For the most prevalent case, which is for uncorrelated noise, the rms value of the noise on the fast-crossover bipolar signal is related to the rms value of the input noise by

$$\sigma_{V(fz)} = \sigma_V \sqrt{2} \qquad (17)$$

Determining the fast-crossover time jitter from Equation (15) also requires knowledge of the slope of the composite timing signal at crossover. The slope of the fast-crossover bipolar signal at zero-crossing time is less than the slope of the leading edge of the delayed anode signal.

For a narrow dynamic range of signal amplitudes, leading-edge timing and TCF timing should both provide less timing error due to noise-induced jitter that the fast-crossover technique. If only the uncorrelated noise is considered, the rms value of the noise is greater on the fast-crossover signal than on either the leading-edge timing signal or the constant-fraction bipolar timing signal.

In addition the slope of the fast-crossover signal at zero crossing is usually less than the slopes of either the leading-edge or the constant-fraction timing signals at their respective pick-off times.

The fast-crossover time pick-off technique can provide excellent time resolution for a wide dynamic range of input signal amplitudes if the signal rise times and fall times do not vary significantly.

The fast-crossover technique has two major advantages and disadvantages. The advantages are: 1) the bipolar signal is simple to form for a specific application because the stub-clipping is passively implemented with a shorted 50-Ω delay line and 2) the zero crossing of the bipolar signal occurs well after the peak of the anode pulse. Thus a leading-edge trigger, used to arm the zero-crossing detector, does not interfere with the timing performance of the instrument. The disadvantages are: 1) for a narrow dynamic range of signals the timing jitter due to noise is greater than it is for either the leading-edge method or the TCF method and 2) changes in pulse shape cannot be tolerated.

CONVENTIONAL CROSSOVER

There are many applications in which a wide range of pulse amplitudes must be handled but optimum time resolution is not required. The linear side channel of a typical fast/slow coincidence system is a good example of this situation (see "Applications"). One solution to this problem is to utilize the zero crossing of the bipolar output signal from a pulse-shaping amplifier to derive timing information and to use the peak amplitude of the unipolar pulse from the amplifier for the energy range information.

Either double-delay-line-shaped pulses or RC-shaped pulses may be used, but the former provide better timing resolution. Timing walk resulting from amplitude variations is essentially reduced to the walk that is due to the charge sensitivity of the zero-crossing detector. The zero-crossing time is still a function of the pulse shape.

Pulse-shaping amplifiers are often designed specifically for energy spectroscopy. The energy information is derived from the peak amplitude of the amplifier's output pulse; thus the shaping filters in the amplifier are set to provide a maximum signal-to-noise ratio. To achieve the best signal-to-noise ratio, a differentiation network that is followed by at least one integration network limits the amplifier bandwidth. Integration significantly increases the rise times of the pulses from the shaping amplifier relative to the rise times of the pulses from the preamplifier. The resulting timing jitter is worse for techniques that derive timing information from the shaping amplifier signal than for the time pick-off techniques that derive timing information from the leading edge of the preamplifier signal.

A comparison of leading-edge timing and conventional crossover timing can be made for scintillation detectors. A double-delay-line-shaped signal with no accompanying integration is used for the bipolar timing pulse in the analysis. The effective triggering fraction for this shaping method is approximately 50% of the collection time, with the rms value of the noise on the bipolar signal approximately twice that at the input. Compared to optimized leading-edge timing at 1-MeV the conventional crossover technique is theoretically shown to be 13.7 times worse for NaI(Tl) and 1.9 times worse for fast plastic scintillators.

The conventional crossover technique is an attractive method for timing with a wide range of signal amplitudes if the best possible timing resolution is not required. This technique is used widely in timing-single-channel analyzers (TSCAs) because the zero crossing occurs well after peaking time of the input signal.

TRAILING EDGE, CONSTANT FRACTION

As was discussed in the preceding section, timing information can be obtained from the slow linear signals that are produced by the pulse-shaping amplifier in the energy spectroscopy system. The timing resolutions obtained from these signals is generally not as good as the resolution obtained from the leading-edge of signals from a fast-timing amplifier. However, the resolution obtained from the slow linear signals is entirely adequate in many of the cases that involve a wide range of signal amplitudes.

A trailing-edge constant-fraction technique can be used with either unipolar or bipolar signals to derive a time pick-off pulse after the peak time of the signal from the shaping amplifier. This technique is extremely useful when incorporated in TSCAs and is illustrated in Figure 13. The linear input signal is stretched and attenuated and then used as the reference level for a timing comparator. The time pick-off signal is generated when the trailing edge of the linear input signal crosses back through the fraction reference level. The fraction, f, is the fraction of amplitude decay toward the baseline as measured from the peak of the input pulse. The amplitude-dependent time walk of the pick-off point is ideally reduced to the time walk associated with the charge sensitivity of the timing comparator. However, the time of occurrence of the pick-off signal is dependent on the shape of the input signal. Resolution can be optimized by careful experimentation with the fraction reference level.

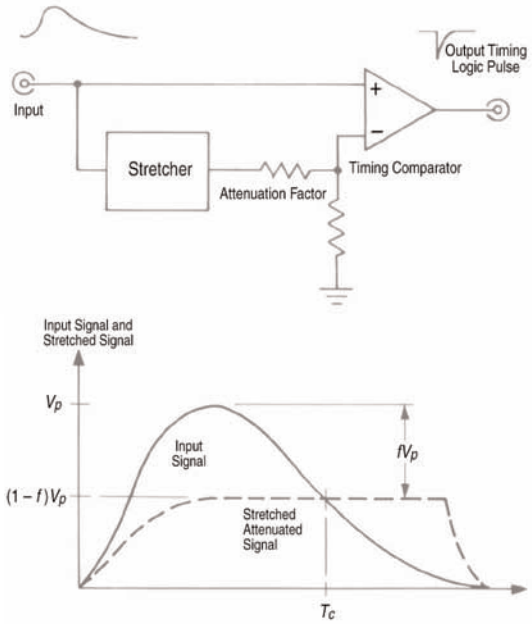

Fig. 13. Signal Formation for Timing with the Trailing-Edge Constant-Fraction Technique.

APPLICATIONS

CONSTANT-FRACTION TIMING WITH SCINTILLATORS

Figure 14 shows a typical fast/slow timing coincidence system that can be use for timing with fast scintillators and PMTs. An integral model constant-fraction discriminator is used as the time pick-off device in each channel leading to the TAC, The model 583B CFD can be operated as an integral discriminator or as a differential discriminator. An energy side channel is associated with each detector and is composed of a preamplifier, a shaping amplifier, and an SCA. The function of the SCA is to select the range of energies for which timing information is desired. If two detected events fall within the selected energy ranges, and if they are coincident within the resolving time selected for the coincidence unit, the precise timing information related to these events is strobed from the TAC. The timing information is accumulated and displayed by the MCA.

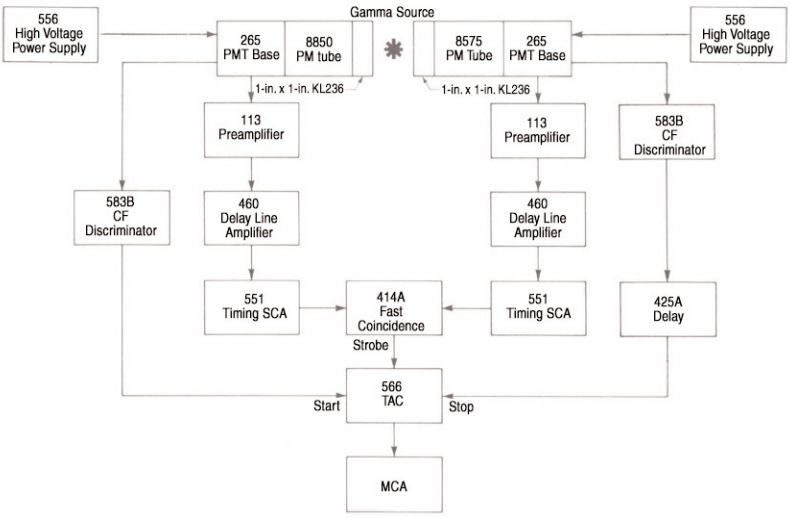

Fig. 14. Typical Fast/Slow Timing sytem for Gamma-Gamma Coincidence Measurements with Scintilators and Photomultiplier Tubes.

The TAC in Figure 14 must handle the count rate associated with the single events exceeding the thresholds of the timing discriminators. This count rate can be an order of magnitude higher than the coincidence rate at which the TAC is strobed. Thus, the TAC imposes a count rate limitation in a fast/slow coincidence system. Resolution degradation can occur at high conversion rates in the TAC due to heating effects in the active circuitry and dielectric absorption in the storage capacitors.

Figure 15 shows a timing coincidence system that performs the same function as the fast/slow system shown in Figure 14. In the system shown in Figure 15, each constant-fraction differential discriminator generates the timing information and determines the energy range of interest simultaneously. If two detector events fall within the selected energy ranges, and if they are coincident within the resolving time selected for the coincidence unit, the TAC is gated on to accept the precise timing information. Thus, the TAC must handle start-stop signals only for events that are of the correct energy and that are coincident. Compared to the fast/slow system, the fast system has fewer modules and improved count rate capability. The system shown in Figure 15 is similar to the fast-fast (F^2) timing coincidence system.

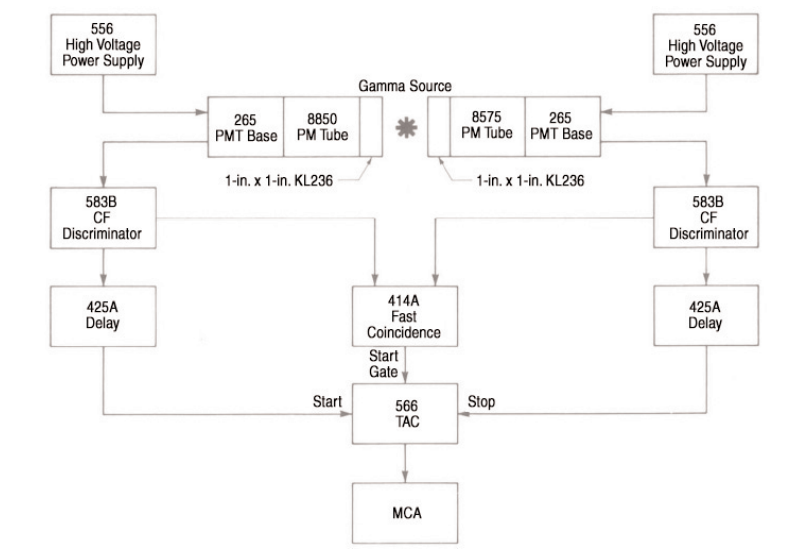

Fig. 15. A Fast-Timing Coincidence System for Gamma-Gamma Coincidence Measurements with Scintillators and Photomultiplier Tubes.

Timing resolution was accumulated for two constant-fraction differential discriminators (INT mode) employed in the fast/slow coincidence system shown in Figure 14. Figure 16 shows the resulting timing resolution with ^{60}Co as a function of the dynamic range of the input signals. The FWHM timing resolution ranges from 189-picoseconds for a 1.1:1 dynamic range of signals to 336-picoseconds for a 100:1 dynamic range. The upper-energy limit used in this experiment was 1.6-MeV.

Timing resolution was also obtained for two constant-fraction differential discriminators (DIFF mode) employed in the simplified, fast-timing coincidence system shown in Figure 15. Figure 17 shows the resulting timing resolution with ^{60}Co as a function of the dynamic range of the input signals. The FWHM timing resolution ranges from 190-picoseconds for a 1.1:1 dynamic range to 337-picoseconds for a 100:1 dynamic range. The upper-energy limit for this experiment was 1.6-MeV. The data obtained with the fast coincidence system was within 5% of that obtained with the fast/slow coincidence system.

Timing resolution as a function of energy is another parameter in characterizing a timing system. Data was obtained for the fast-timing coincidence system using ^{60}Co and maintaining 100-keV energy windows with the differential discriminators. The resulting timing data is displayed in Figure 18. Each axis represents the energy levels selected by the respective differential discriminator. The data included in each rectangle of the array is the FWHM, FWTM, and FW(1/100)M system timing resolution for the coincidence of the two selected energy ranges. The system FWHM timing resolution ranges from 176-picoseconds for 950-keV to 1050-keV windows on both channels, from 565-picoseconds for 50-keV to 150-keV windows on both channels.

Figure 19 is a plot of the timing resolution as a function of energy for each differential discriminator timing channel in the fast-timing coincidence system. Data points for this plot were obtained from the information along the diagonal array in Figure 18, assuming equal contributions form each channel. The FWHM resolution for each channel ranges from 124-picoseconds at 1-MeV to 400-picoseconds at 100-keV.

Figure 20 is a plot of the output rate of the coincidence unit used in the two timing system as a function of the input data rate. The coincidence resolving time was set at 50-nanoseconds for both the fast and fast/slow systems. In the fast-timing system, the coincidence output signals are used to gate the TAC for valid start signals, and the coincidence output rate shows a linear relationship to the input data rate. In the fast/slow system, the coincidence output signals are used to strobe the timing information from the TAC. The plot for the fast/slow system in Figure 20 shows a marked decrease in the coincidence output rate for input data rates exceeding 100-kcps. This decrease in coincidence output rate results in a direct decrease in TAC output rate for corresponding input data rates. The decrease in coincidence efficiency in the fast/slow system is attributable to pile-up effects and baseline movement of the main shaping amplifiers at these high data rates. At an input data rate of 200-kcps, the fast system showed a factor-of-6 improvement in coincidence rate.

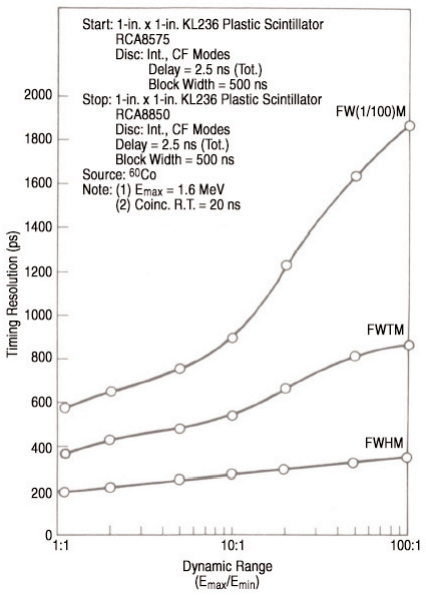

Fig. 16. Timing Resolution as a Function of Dynamic Range for Two Constant-Fraction Differential Disciminators in a Fast/Slow Timing Coincidence System.

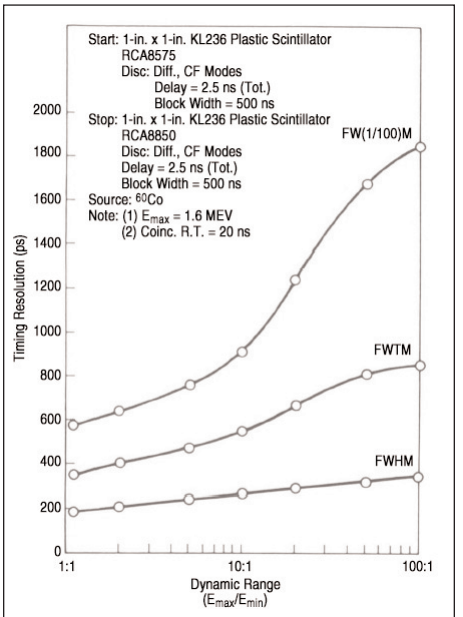

Fig. 17. Timing Resolution as a Function of Dynamic Range for Two Constant-Fraction Differential Discriminators in a Fast Timing Coincidence System.

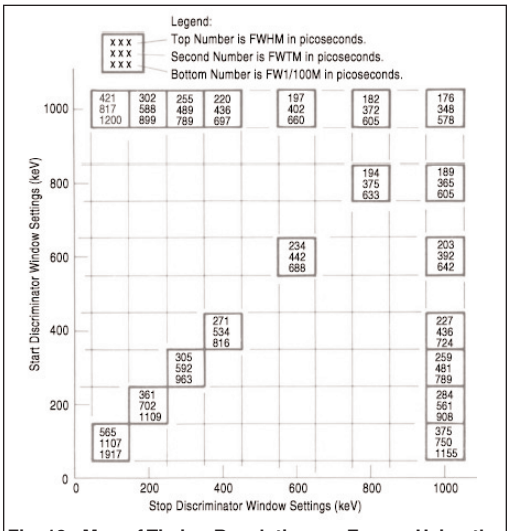

Fig. 18. Map of Timing Resolution vs. Energy Using the Fast-Timing Coincidence System with a 1-in. x 1-in KL236 Scintillator and ^{60}Co.

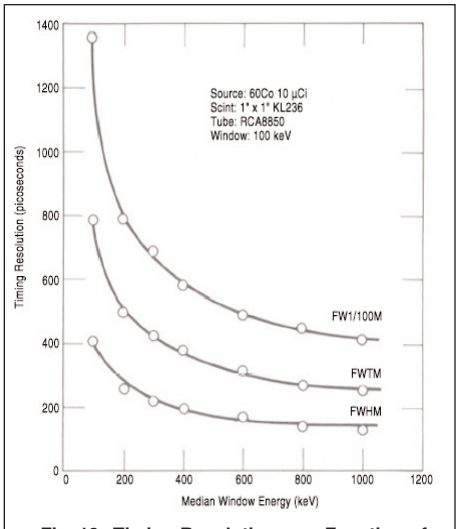

Fig. 19. Timing Resolution as a Function of Energy for Each Differential Discriminator Timing Channel in the Fast-Timing System.

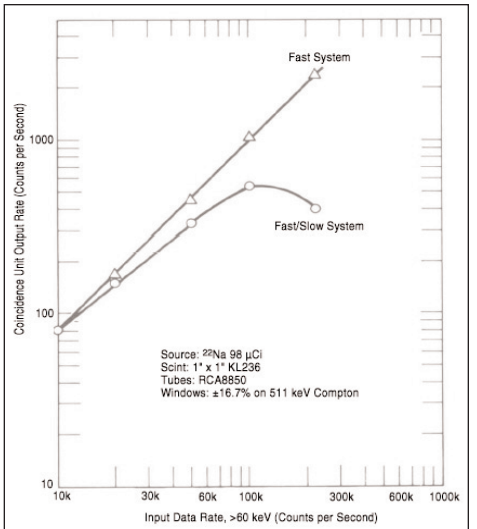

Fig. 20. Timing Coincidence Output Rate as a Function of Input Data Rate.

The fast/slow timing coincidence system and the fast-timing coincidence system can also be used with NaI(Tl) scintillators. A unique problem encountered with NaI(Tl) scintillators is their long decay time ($\tau \cong 250$ ns). Individual photoelectron events near the trailing edge of the NaI(Tl) pulse can produce spurious timing output signals from the constant-fraction discriminator. This problem can be overcome by selecting the proper discriminator and adjusting the dead time that is comparable to the pulse width of the NaI(Tl) signal. Figure 21 is a plot of a time resolution versus dynamic range for an NaI(Tl) detector that is mounted on an RCA 8575 PMT. The system is similar to that shown in Figure 14 but with the NaI(Tl) detector used in the stop channel and a KL236 plastic scintillator used to trigger the start channel.

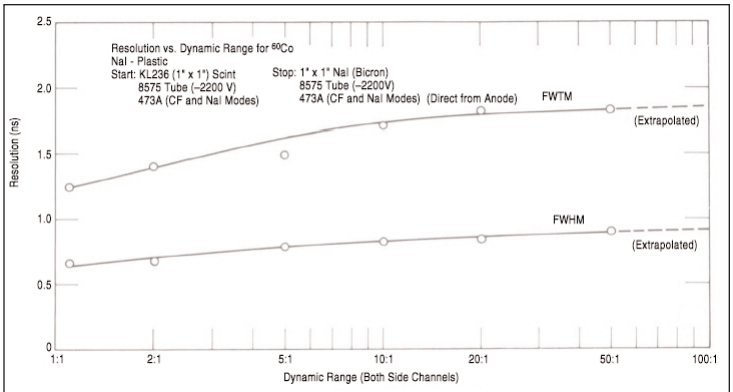

Fig. 21. Plot of Time Resolution vs. Dynamic Range Using NaI(Tl) Detectors, RCA 8575 PMTs, and a CFD.

Some timing spectroscopy applications involve very high data rates. The ORTEC model 935 is a Quad Constant-Fraction Discriminator capable of resolving pulses separated by less than 10-nanoseconds. Figure 22 (a), (b), and (c) depict the response of the Model 935 to a burst of five pulses less than 10-nanoseconds apart. Other models can resolve from 20-nanoseconds to about 50-nanoseconds of separation between pulses.

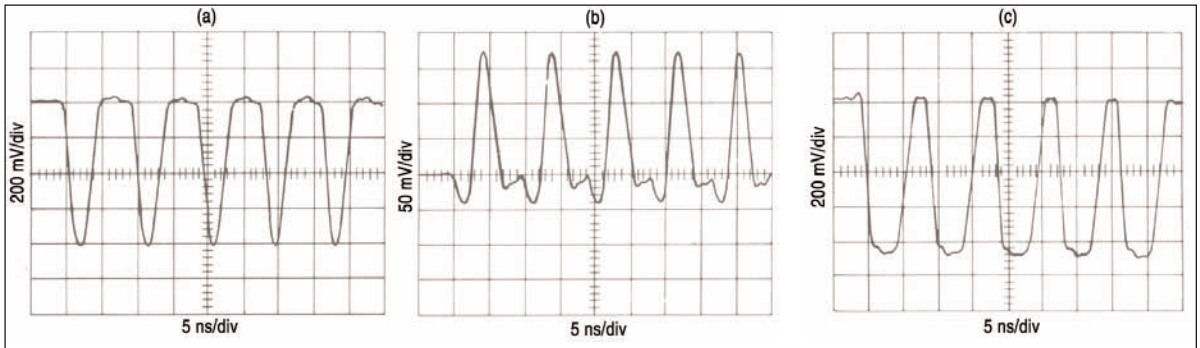

Fig. 22. (a) Input Signal Burst of 5 Pulses to the CFD. (b) Constant-Fraction Zero-Crossing Monitor Signal for the Burst Input. (c) Constant-Fraction Discriminator Output Burst Response. (CF delay = 1.5 ns; threshold = 30 mV.)

Proper adjustment of the delay and walk are critical for excellent timing resolution. With scintillators, the CFD is usually operated in the true-constant-fraction mode (TCFF) described earlier. The shaping delay is chosen to cause the zero crossing of the constant-fraction signal to occur just after the peak of the attenuated input signal. Figure 23 (a) shows a signal representative of the output from a fast PMT. Figure 23(b) shows the CF monitor signal for a properly chosen delay of about 1.5-nanoseconds.

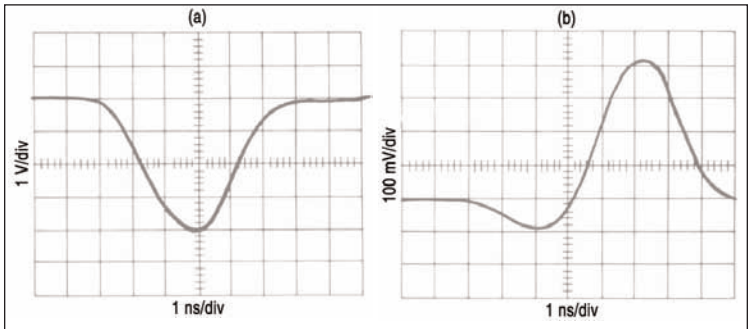

Fig. 23. (a) Input Signal Shape for Time Walk Measurements Near Threshold. (b) Constant-Fraction Monitor Signal for the Input Signal Shown Above. (CF delay = 1.5 ns total.)

Proper walk adjustment is also important. Figure 24(a) shows the output signal from the anode of an RCA 8850 PMT. Figures 24(b) and (c) show the corresponding CF monitor signal as seen on a sampling oscilloscope triggered by the discriminator output signal. The walk is adjusted to minimize the time spread of the zero-crossing point.

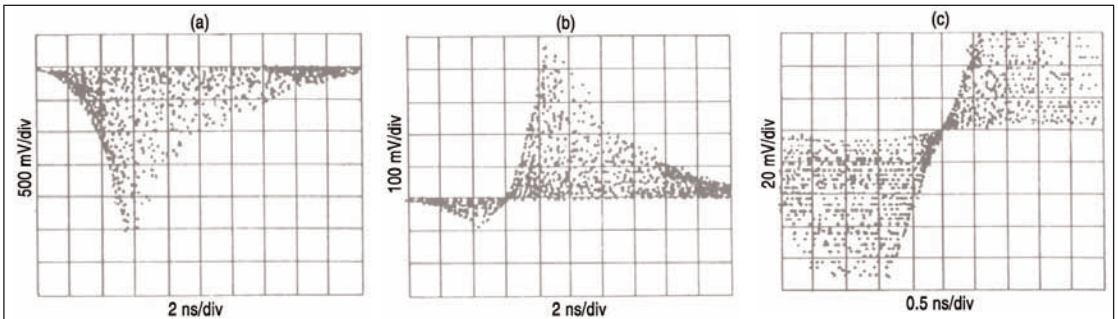

Fig. 24. (a) RCA 8850 PMT Anode Signal with a 1-in. x 1-in. KL236 Scintillator and ^{60}Co. (b) Constant Fraction Zero-Crossing Monitor Signal, Triggered by the Discriminator Output for the Anode Signal Shown Above. (c) Expanded View of the Constant-Fraction Zero-Crossing Monitor Signal. (CF delay = 3 ns; threshold = 30 mV.)

CONSTANT-FRACTION TIMING WITH GERMANIUM DETECTORS

A timing spectroscopy system suitable for use with germanium detectors is shown in Figure 25. The start signal for the TAC is derived from a fast scintillator and PMT. The stop signal is derived from the germanium detector charge-sensitive preamplifier with additional shaping by the timing-filter amplifier (TFA). Timing data is strobed from the TAC by a TSCA set on the energy range of interest. The start CFD threshold was set at 150-keV. The preamplifier and amplifier connected to the dynode of the PMT are used to set the start CFD threshold. The system timing resolution was 176-picoseconds per channel measured with a time calibrator. The timing properties of a series of 14-detector-preamplifier combinations were measured. Detector data is shown in Table 1. The initial step in optimization of the timing spectrometer for a given detector was to vary the stop CFD delay to determine it's optimum value. A typical set of data is shown in Figure 26 for Detector No. 7. In general, the FWHM curve shows a shallow minimum and the FWTM curve a more pronounced minimum. An optimum delay of 24-nanoseconds was selected.

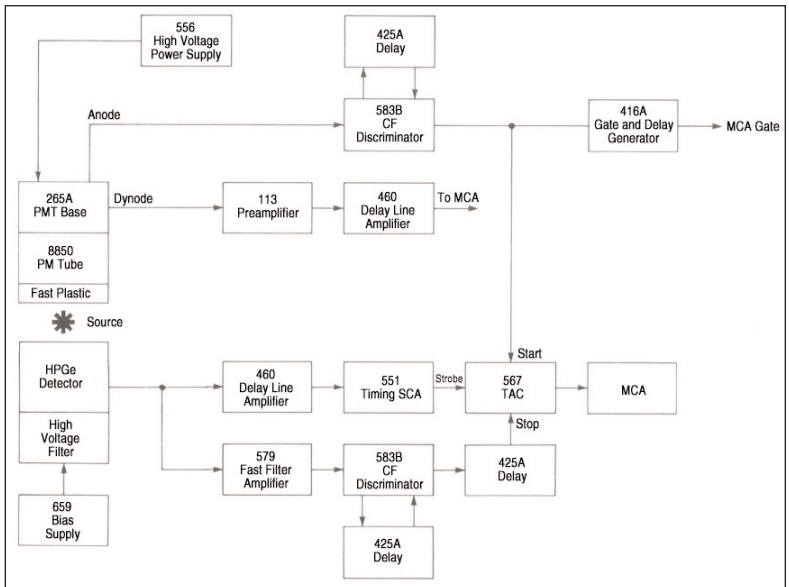

Fig. 25. Block Diagram of Timing Spectrometer.

Timing resolution also depends on the settings of the TFA and type of CFD used. Figure 27 shows timing resolution FWHM and FWTM as a function of the CFD type and TFA time constant. CFD-1 uses a passive mixing technique to form the constant-fraction signal and has a much broader bandwidth than CFD-2 which uses active mixing in an ECL line receiver. The best time resolution was obtained using CFD-1 and the minimum integration time constant on the TFA.

The threshold setting on the CFD in the germanium detector signal-processing chain has an important effect on timing resolution. Setting the threshold too low can result in triggering the CFD on noise and broadening the timing spectrum on the early or left side. Setting the threshold too high can result in leading-edge timing an broadening the spectrum on the late or right side. These effects are shown in Figure 28 for Detector No. 9. During this series of tests the TSCA was set at 511 ±50 keV. Typically, the FWHM improves for threshold settings up to approximately 35% of the energy of interest while the minimum FWTM occurs for a threshold setting of approximately 15% of the energy of interest.

The tests described form the basis for optimizing the germanium detector timing spectrometer for measurements as a function of energy. The TFA was set at minimum integration and the gain was set so the 511-keV line of the ^{22}Na produced approximately a 1-V pulse. The stop CFD threshold was set at 50-keV. The TSCA window was set at 100-keV and data was taken for energies ranging from 150 ±50 keV to 511 ±50 keV using ^{22}Na. Additional data was taken using ^{60}Co for energies ranging from 511 ±50 keV to 1330 ±50 keV. The timing data is summarized in Table 2.

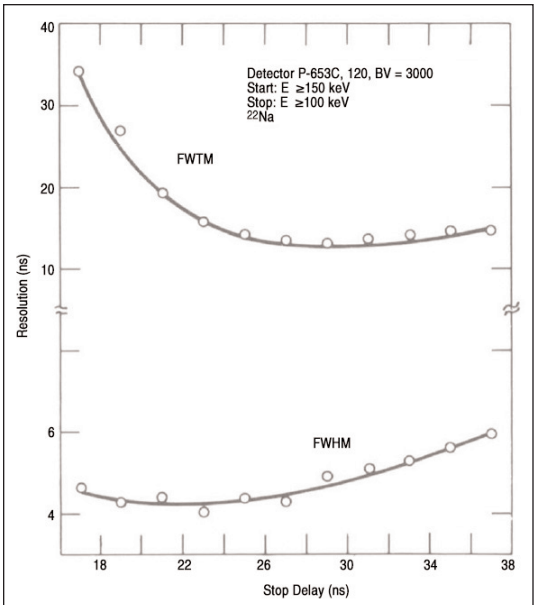

Fig. 26. Timing Resolution FWHM and FWTM as a Function of Constant-Fraction Shaping Delay.

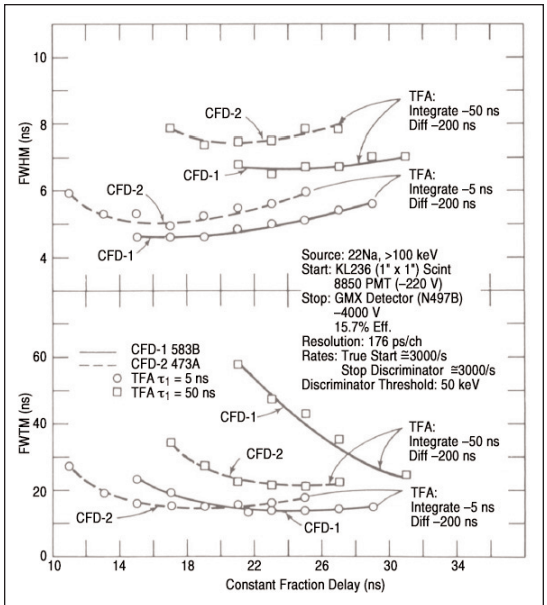

Fig. 27. Timing Resolution FWHM and FWTM as a Function of CFD Type and TFA Time Constant.

Table 1. Detector-Preamplifier System Characteristics.

Detector System	Preamp Type	Detector Type	Serial No.	Efficiency (%)	Diameter (mm)	Length (mm)	Core in Hole (mm)	Resolution at 1.33 MeV (keV)	Pulser Resolution at 1.33 MeV (eV)	Depletion Voltage (V)	Bias (V)	Peak-to-Compton	Depth of Hole (mm)
1	Discrete	HPGe-P	P-13ZB	17.7	48	52.1	8	1.66	620	1800	+3000	59.0	37.2
2	Hybrid	HPGe-P	P-13ZB	17.7	48	52.1	8	1.64	590	1800	+3000	59.0	37.2
3	Discrete	HPGe-P	P-353	13.2	43	53.3	8	1.66	600	1800	+3000	51.8	39.9
4	Hybrid	HPGe-P	P-589	19.5	50	50.9	8	1.77	560	1500	+3500	55.7	32.6
5	Hybrid	HPGe-P	P-621	28	53.3	60.8	8	1.87	730	2400	+3500	70.9	45.8
6	Discrete	HPGe-P	P-633	22.5	48.6	64.8	8	1.85	660	2500	+3500	58.1	50.2
7	Discrete	HPGe-P	P-653C	11.0	45.6	36.3	8	1.61	510	1900	+3000	49.2	21.4
8	Hybrid	HPGe-P	P-654A	17.1	47.9	50.9	8	1.65	630	2200	+3500	55.9	35.7
9	Discrete	HPGe-P	P-9000	35	57	64	8	1.77	842	1500	+3500	69.6	52
10	Discrete	HPGe-N	N-491B	12.5	43.6	46	8	1.69	690	–1000	–3500	48	37.6
11	Discrete	HPGe-N[1]	N-492B	11.6	44.1	38.2	8	1.73	506	–1700	–2000	46	29
12	Discrete	HPGe-N	N-497B	15.7	46.5	48.5	8	1.84	550	–2200	–4000	45	40
13	Discrete	HPGe-N	N-529	19.8	48.1	54.8	8	1.99	760	–1200	–2000	47.7	51
14	Hybrid	HPGe-N	N-627B	16.4	46.7	48.4	8	1.73	506	–1000	–1800	53.4	39.1

[1]Be Window

Table 2. Timing Resolution as a Function of Energy for an Energy Window of ±50 keV.

Detector System	Detector Type	Efficiency (%)	Optimum Delay (ns)	Measure	Timing Resolution (ns)								
					Mean Energy (keV) Using ^{22}Na				Mean Energy (keV) Using ^{60}Co				
					150	250	350	511	511	750	950	1170	1330
1	HPGe-P	17.7	31	FHWM FWTM	10.2 —	6.9 53.7	5.9 24.8	4.4 10.2	4.8 10.6	4.1 9.3	3.7 9.0	3.0 7.5	2.5 6.7
2	HPGe-P	17.7	26	FHWM FWTM	9.2 —	6.9 41.2	5.6 12.8	4.2 9.0	4.2 9.9	3.7 8.6	2.8 7.6	2.6 6.0	2.2 5.8
3	HPGe-P	13.2	32	FHWM FWTM	9.5 —	6.5 37.3	5.9 20.6	4.4 10.0	5.0 10.9	4.0 9.9	3.3 9.4	2.8 7.7	2.7 7.2
4	HPGe-P	19.5	33	FHWM FWTM	8.8 —	7.0 57.5	5.9 31.7	4.3 10.7	5.0 11.8	3.9 10.4	3.7 9.9	2.8 7.6	2.6 7.0
5	HPGe-P	28	34	FHWM FWTM	11.3 —	8.8 55.8	7.7 27.1	5.6 12.8	6.2 13.4	5.7 12.3	4.0 11.8	3.6 9.8	3.4 9.0
6	HPGe-P	22.5	36	FHWM FWTM	— —	39.0	14.2 100	6.7 21.1	7.4 36.6	5.7 16.9	4.5 10.9	4.0 8.8	3.7 8.4
7	HPGe-P	11.0	24	FHWM FWTM	9.2 —	6.7 45.3	5.8 22.2	4.0 9.9	3.9 10.2	3.0 8.4	2.6 7.5	2.0 5.6	1.7 5.1
8	HPGe-P	17.1	36	FHWM FWTM	10.0 —	7.7’ 26.0	6.5 16.4	4.6 11.3	5.1 13.2	4.0 12.5	3.5 11.6	3.0 9.7	2.5 8.8
9	HPGe-P	35	25	FHWM FWTM	— —	11.8 62	11.0 34	8.2 25	9.0 45	6.2[5] 17[5]	5.6 18.5	4.8 15.3	— —
10	HPGe-N	12.5	24	FHWM FWTM	9.9 66.2	7.6 28.2	6.0 15.8	4.6 10.0	4.6 11.4	3.3 9.2	2.64 7.4	2.6 7.0	2.0 5.1
11	HPGe-N[1]	11.6	23	FHWM FWTM	8.0 78	5.9 27.5	4.7 12.3	3.6 7.9	3.5 8.8	2.8 6.7	2.1 5.8	1.9 4.6	1.6 4.1
12	HPGe-N	15.7	23	FHWM FWTM	10.7[4] —	7.2[4] 41[4]	5.8[4] 15[4]	4.4 10.4	4.1 11	2.8[5] 8.1[5]	— —	2.1 5.8	— —
13	HPGe-N	19.8	23	FHWM FWTM	12.5 84	8.6 33	7.0 18.1	4.5 10.2	4.9 11.8	3.7 8.6	3.1 7.7	2.2 5.5	2.0 4.9
14	HPGe-N	16.4	24	FHWM FWTM	8.6 77.3	6.7 22.5	5.6 16.2	4.1 9.7	4.2 10.7	3.1 8.1	2.7 7.4	2.3 5.5	2.0 5.1

[1] Operated at 1900 V
[2] Operated at 4800 V
[3] Operated at 2300 V
[4] 60-Co
[5] 800 keV

A plot of timing resolution FWHM and FWTM is shown in Figure 29 for Detector no. 11. Leading edge walk is evident in the FWTM resolution for mean energies less than approximately 400 keV.

One comparison between the detector is shown in Figure 30 where the timing resolution at FWHM is plotted versus detector relative efficiency for the energy 511 ± 50 keV using ^{22}Na. A possible conclusion is that larger detectors tend to have poorer timing performance.

Many discriminators include the Slow Rise Time Reject (SRT) operational mode as well as constant fraction and leading edge. The function of the SRT circuitry is to eliminate leading-edge walk, a common occurrence in germanium timing systems. This leading-edge walk results from the wide spread of rise times that result from the charge collection time variations within the germanium crystal. The SRT circuitry is most effective when used with a wide dynamic range of energies. Figure 31 shows the dramatic improvement at even the FW(1/100)M level. The SRT circuitry provides this improvement in timing resolution by rejecting the timing output pulses that result from leading-edge timing. Since the input signals that cause leading-edge walk represent valid energy information, use of the SRT circuitry results in a loss in the counting efficiency of the system.

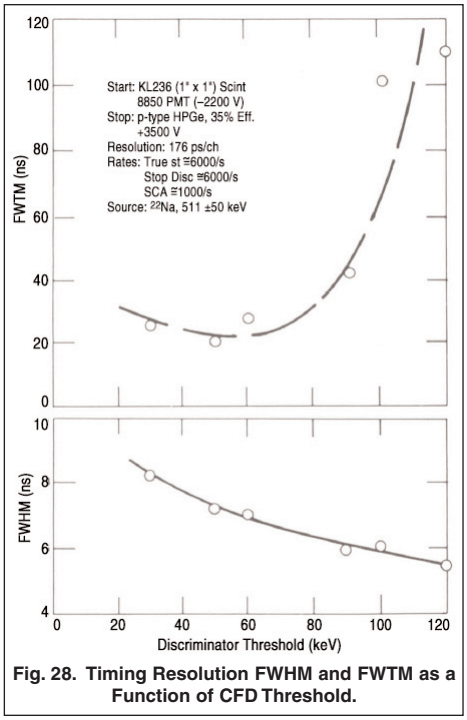

Fig. 28. Timing Resolution FWHM and FWTM as a Function of CFD Threshold.

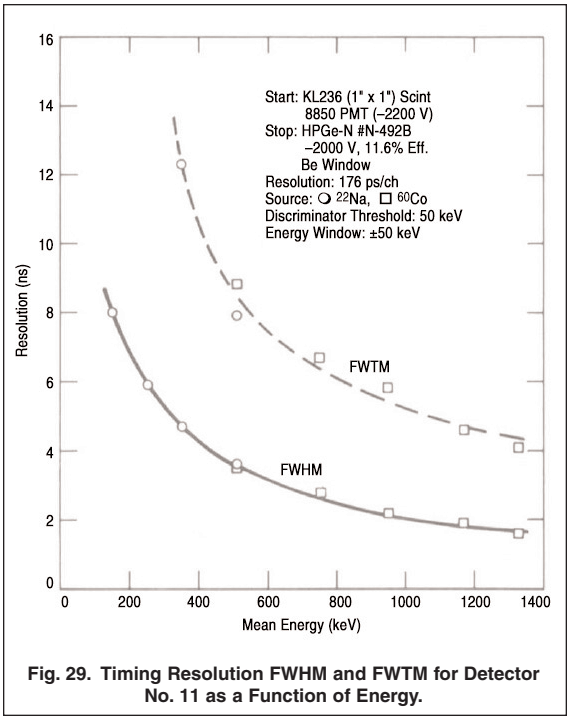

Fig. 29. Timing Resolution FWHM and FWTM for Detector No. 11 as a Function of Energy.

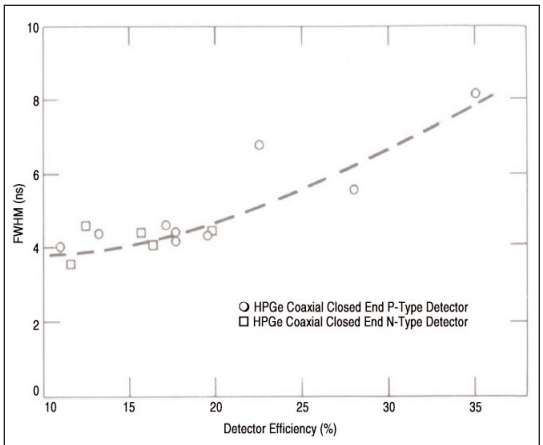

Fig. 30. Timing Resolution FWHM for 14 Detector Systems as a Function of Efficiency for the Energy Range 511 ± 50 keV for ^{22}Na.

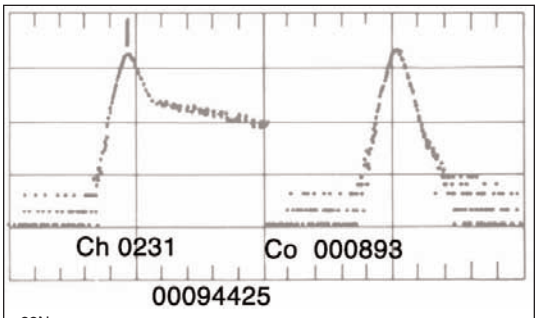

22Na
Start: KL236, RCA8575 Photomultiplier Tube
Stop: Ge Coaxial Detector, 12.5%, 62.3 cc
10:1 Dynamic Range

	CF	SRT
FWHM	4.5 ns	4.4 ns
FWTM	13.2 ns	9.4 ns
FW1/100M	—	17.3 ns

Fig. 31. Timing Spectrum for a Wide Dynamic Range (10:1).

Low Energy Photon (LEPS) detectors are also used in timing applications. Typical timing resolution for a 6-mm diameter LEPS system is shown in Figure 32.

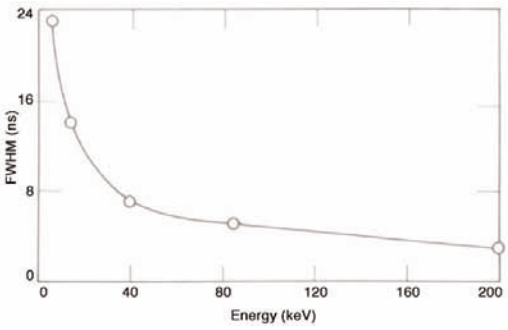

Fig. 32. Time Resolution vs Energy for a 6-mm LEPS Detector.

TIMING WITH SINGLE-CHANNEL ANALYZERS

As discussed in the sections "Conventional Crossover" and "Trailing Edge, Constant Fraction", some applications do not require the ultimate in timing resolution performance. Therefore a separate timing channel can be eliminated and adequate timing data can be obtained from an SCA used in an energy spectroscopy system. The total system cost and complexity can be reduced in the timing resolution obtainable from the TSCA is adequate for the particular application.

Figure 33 is a block diagram of a system that can be used to determine the timing characteristics of an SCA with a germanium detector. In this system the timing resolution is almost entirely dominated by the resolution of the channel that includes the germanium detector and the TSCA.

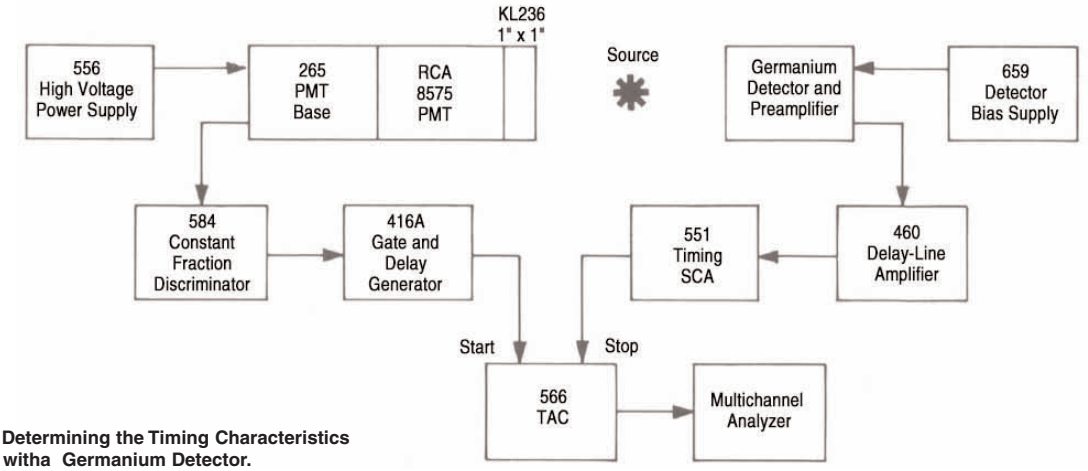

Fig. 33. Typical System for Determining the Timing Characteristics of an SCA Used witha Germanium Detector.

Figure 34 is a plot of timing resolution versus dynamic range for two types of detectors used in a system similar to the one shown in Figure 33. Resolution curves are shown for the trailing-edge constant-fraction time pick-off techniques. Double-delay-line clipping shaped the bipolar signals used for timing. The timing resolution obtained by this technique can be worse by approximately an order of magnitude than the resolution obtained by the optimum constant-fraction technique discussed earlier.

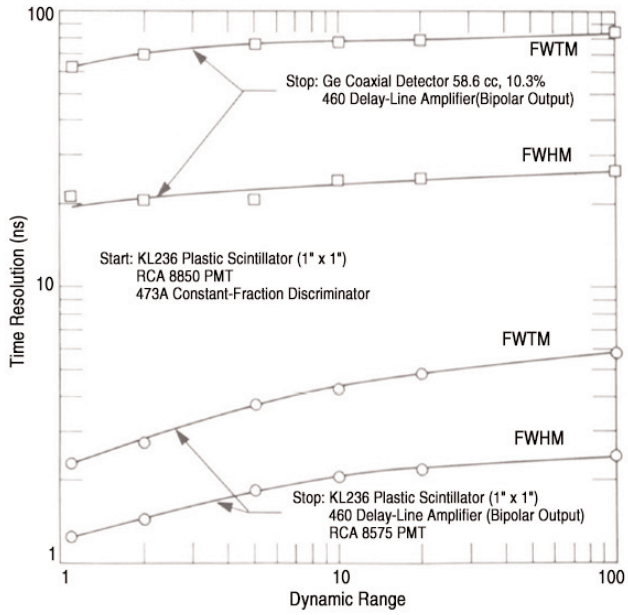

Fig. 34. Timing Resolution vs Dynamic Range, E_{max}/E_{min}, Where E_{max} is 1.6 MeV for the ORTEC 551 Timing SCA Using the Trailing-Edge Constant-Fraction Technique.

TIMING WITH SURFACE-BARRIER DETECTORS

A surface-barrier detector is fundamentally a large-area p-n junction diode, consisting of an extremely thin p-type layer on an n-type silicon wafer. It can be used in the detection of low-mass charged particles, fission fragments, and light signals in a wide variety of applications. The relatively short charge collection times in a surface-barrier detector allow it to be used in fast-timing experiments.

The system shown in Figure 35 can be used to test a surface-barrier detector and preamplifier timing system. The timing resolution is determined by using a 904-nanometer light pulse that is generated by a laser diode pulser (LDP). Light pulses with sub-nanosecond duration can be obtained in this manner. A simulated timing test can be conducted for almost any equivalent energy level by calibrating the detected light with a weak alpha source placed in the vicinity of the detector. Although the detector response to the LDP is different from it's response to charged particles, the test system and data presented here are useful for aligning and adjusting. Also, the measured timing resolution at a given equivalent energy represents the system timing error due to jitter. Timing resolution for six different surface-barrier detectors is shown in Figure 36.

ORTEC manufactures a series of outstanding preamplifiers for use with surface-barrier detectors. These preamplifiers are optimized for the capacitance of the detectors. These fast rise-time charge-sensitive preamplifier outputs can provide timing outputs by differentiating the energy output from the charge loop. The rise time can be easily adjusted in each application to ensure optimum performance.

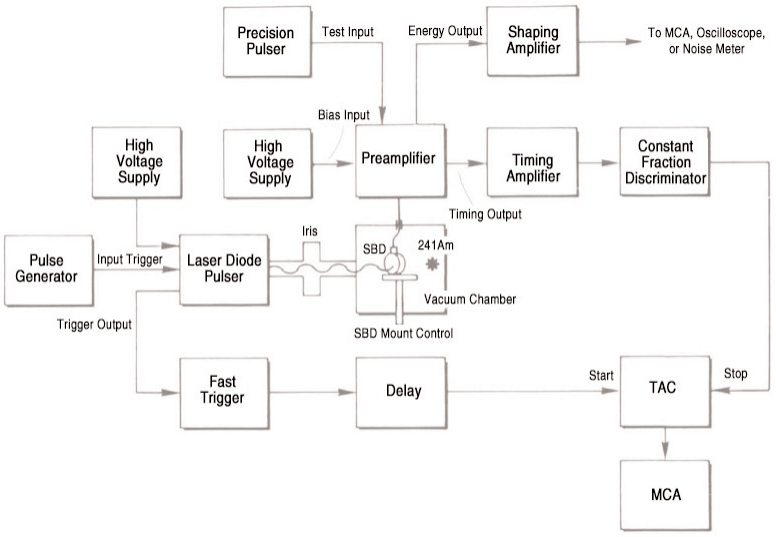

Fig. 35. Block Diagram of the Test System Used for Testing Charged-Particle Detectors with a Laser Diode Pulser.

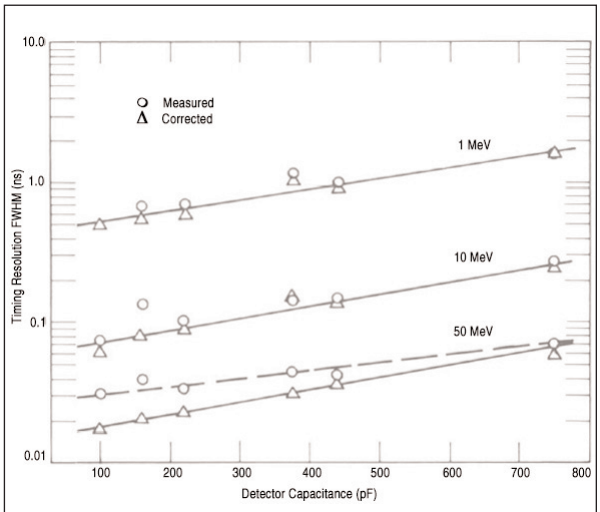

Fig. 36. Timing Resolution vs Energy for Surface-Barrier Detectors. The Measured Data Were Generated by a Pulsed Laser Calibrated to the 5.49-MeV Alpha of ^{241}Am, and the Corrected Data Were Obtained by Subtracting the System Resolution in Quadrature.

Bibliography

A complete listing of all the literature relevant to timing would be prohibitive. Only a few of the important works of some of the major contributors to the state-of-the-art are listed. The interested reader can use this partial listing as a starting point for an in-depth study of any particular aspect of timing. For convenience the references are categorized by application as follows:

Scintillator/Photomultiplier Tube Timing
Germanium Timing
Silicon Surface-Barrier Detector Timing
Photon Counting and Photomultiplier Tubes
General

Scintillator/Photomultiplier Tube Timing

1. A. Schwarzschild, "A Survey of the Latest Developments in Delayed coincidence Measurements," *Nucl. Instrum. Methods* **21**, 1 (1963).
2. E. Gatti and V. Svelto, "Revised Theory of Time Resolution in Scintillation Counters," *Nucl. Instrum. Methods* **30**, 213 (1964).
3. G. Present, A. Schwarzschild, I. Spirn, and N. Wotherspoon, "Fast Delayed Coincidence Technique: The XP1020 Photomultiplier and Limits of Resolving Times Due to Scintillator Characteristics," *Nucl. Instrum. Methods* **31** 71–76 (1964).
4. L. G. Hyman, "Time Resolution of Photomultiplier Systems," *Rev. Sci. Instrum.* **36**, 193 (1965).
5. D. Wieber and H. Lefevre, "An Amplitude-Independent Nanosecond Timing Discriminator for Fast Photomultipliers," *IEEE Trans. Nucl. Sci.* **NS-13** (1), 406 (1966).
6. R. E. Bell, "Comparison of Leading Edge and Crossover Timing in Coincidence Measurements," *Nucl. Instrum. Methods* **42**, 211 (1966).
7. E. Gatti and V. Svelto, "Review of Theories and Experiments of Resolving Time with Scintillation Counters," *Nucl. Instrum. Methods* **43**, 248 (1966).
8. G. Bertolini, M. Cocchi, V. Mandl, and A. Rota, "Time Resolution Measurements with Fast Photomultipliers," *IEEE Trans. Nucl. Sci.* **NS-13**, 119 (1966).
9. W. J. McDonald and D. A. Gedcke, "Time Resolution Studies on Large Photomultipliers," *Nucl. Instrum. Methods* **55** 1 (1967).
10. M. Bertolaccini, C. Bussolati, S. Cova, S. Donati, and V. Svelto, "Statistical Behavior of the Scintillation Counter: Experimental Results," *Nucl. Instrum. Methods* **51**, 325 (1967).
11. D. A. Gedcke and W. J. McDonald, "A Constant Fraction of Pulse Height Trigger for Optimum Time Resolution," *Nucl. Instrum. Methods* **55**, 377 (1967).
12. S. Donati, E. Gatti, and V. Svelto, "An Equivalent Circuit for the Statistical Behavior of the Scintillation Counter," *Nucl. Instrum. Methods* **46**, 165 (1967).
13. B. Vojnovic, "A Subnanosecond Timing Circuit Using Snap-Off Diode," paper 59 in *International Symposium on Nuclear Electronics*, 1968.
14. G. Cariolaro, "The Jitter Caused by Noise in Trigger Circuits," *IEEE Trans. Inf. Theory* **IT-14** (4), 535 (1968).
15. R. Nutt, "A Study of a NaI(Tl) Scintillator/Photomultiplier Timing System," Ph.D. dissertation, The University of Tennessee, Knoxville (1969).
16. Y. K. Akimov and S. V. Medved, "On the Theory of the Resolving Time of Scintillation Counters," *Nucl. Instrum. Methods* **78**, 151 (1970).
17. M. R. Maier and P. Sperr, "On the Construction of a Fast Constant Fraction Trigger with Integrated Circuits and Application to Various Photomultiplier Tubes," *Nucl. Instrum. Methods* **87**, 13 (1970).
18. J. Bialkowski and M. Moszynski, "Timing System for High Resolution Time Spectroscopy," *Nucl. Instrum. Methods* **105**, 51 (1972).
19. R. Nutt, "Detecting Circuit for Indication Occurrence of Peak in an Input Signal," U.S. Patent No. 3,714,464, January 30, 1973.
20. L. A. Eriksson, C. M. Tsai, Z. H. Cho, and C. R. Hurlbut, "Comparative Studies on Plastic Scintillators — Applications to Low Energy High Rate Photon Detection," *Nucl. Instrum. Methods* **122**, 373 (1974).
21. P. B. Lyons and J. Stevens, "Time Response of Plastic Scintillators," *Nucl. Instrum. Methods* **114**, 313 (1974).
22. J. Bialkowski, Z. Moroz, and M. Moszynski, "Further Study of Timing Properties of Scintillation Counters," *Nucl. Instrum. Methods* **117**, 221 (1974).
23. M. I. Green, P. F. Kenealy, and G. B. Beard, "Fast-Timing Measurements Using a Chevron Microchannel Plate Electron Multiplier," *Nucl. Instrum. Methods* **126**, 175 (1975).
24. C. Cernigoi, N. Grion, and G. Pauli, "Timing with Large Area Plastic Scintillator Counters," *Nucl. Instrum. Methods* **131**, 495 (1975).
25. W. H. Hardy, II, and K. G. Lynn, "A New Approach to Timing: The Fast-Fast System," *IEEE Trans. Nucl. Sci.* **NS-23**, 229 (1976).
26. M. Moszynski, "Study of Light Collection Process from Cylindrical Scintillators," *Nucl. Instrum. Methods* **134**, 77 (1976).
27. S. Sanyal, S. C. Pancholi, and S. L. Gupta, "Sub-Nanosecond Timing Studies with Plastic Scintillation Detectors," *Nucl. Instrum. Methods* **136**, 157 (1976).

28. P. B. Lyons, C. R. Hurlbut, and L. P. Hocker, "Sub-Nanosecond Plastic Scintillators," *Nucl. Instrum. Methods* **133**, 175 (1976).
29. M. Moszynski and B. Bengtson, "Light Pulse Shapes from Plastic Scintillators," *Nucl. Instrum. Methods* **142**, 417–434 (1977).
30. J. D. McGervey, J. Vogel, P. Sen, and C. Knox, "Time Resolution Measurements with an Improved Discriminator and Conical Scintillators," *Nucl. Instrum. Methods* **143**, 435–439 (1977).
31. M. O. Bedwell and T. J. Paulus, "A Versatile Constant Fraction 100-MHz Discriminator," *IEEE Trans. Nucl. Sci.* **NS-25** (1), 86 (1978).
32. B. Bengtson and M. Moszynski, "Study of Primary Energy Transfer Process in Ultrafast Plastic Scintillators," *Nucl. Instrum. Methods* **155**, 221–231 (1978).
33. M. Moszynski, "Light Pulse Shape Study From Crystal Organic Scintillators," *Nucl. Instrum. Methods* **153**, 439–443 (1978).
34. M. O. Bedwell and T. J. Paulus, "A Constant Fraction Differential Discriminator for Use in Fast Timing Coincidence Systems," *IEEE Trans. Nucl. Sci.* **NS-26** (1), 442 (1979).
35. M. Moszynski and B. Bengtson, "Status of Timing with Plastic Scintillation Detectors," *Nucl. Instrum. Methods* **158**, 1–31 (1979).
36. H. Murayama, E. Tanaka, and N. Nohara, "A New Method for Measuring the Statistical Resolution of Scintillation Detectors," *Nucl. Instrum. Methods* **164**, 447–451 (1979).
37. M. O. Bedwell and T. J. Paulus, "A New High Rate Positron Lifetime Measurement System," Proceedings of the Fifth International Conference on Positron Annihilation, Lake Yamanaka, Japan, 375 (April 1979).
38. G. H. Sanders, G. W. Hart, G. E. Hogan, J. S. Frank, C. M. Hoffman, H. S. Matis, and V. D. Sandberg, "A High Performance Timing Discriminator," *Nucl. Instrum. Methods* **180**, 603–614 (1981).
39. G. J. Wozniak, L. W. Richardson, and M. R. Maier, "Time-Walk Characteristics of an Improved Constant Fraction Discriminator," *Nucl. Instrum. Methods* **180**, 509–510 (1981).
40. M. Moszynski, C. Gresset, J. Vacher, and R. Odru, "Timing Properties of BGO Scintillator," *Nucl. Instrum. Methods* **188**, 403–409 (1981).

Germanium Timing

41. P. R. Orman, "A Synchronizing Discriminator for Scintillation Counter Pulses," *Nucl. Instrum. Methods* **21**, 121 (1963).
42. E. Sakai, "Charge Collection in Coaxial Ge(Li) Detectors," *IEEE Trans. Nucl. Sci.* **NS-15** 310 (1968).
43. R. L. Chase, "Pulse Timing System for Use with Gamma Rays on Ge(Li) Detectors," *Rev. Sci. Instrum.* **39**(9), 1318 (1968).
44. E. Sakai, T. A. McMath, and R. G. Franks, "Further Charge Collection Studies in Coaxial Ge(Li) Detectors," *IEEE Trans. Nucl. Sci.* **NS-16**, 68 (1968).
45. T. D. Douglass, "The Application of Filters to Time Analysis of Signals from Ge(Li) Detectors," Ph.D. dissertation, The University of Tennessee, Knoxville (1968).
46. Z. H. Cho and R. L. Chase, "Comparative Study of the Timing Techniques Currently Employed with Ge Detectors," *Nucl. Instrum. Methods* **98**, 335–347 (1972).
47. Z. H. Cho and R. L. Chase, "Improved Amplitude and Rise Time Compensated Timing wth Ge Detectors," *IEEE Trans. Nucl. Sci.* **NS-19**(1), 451 (1972).
48. M. Moszynski and B. Bengtson, "The Shape Distribution of Pulses from Planar Ge(Li) Detector Studies by a Differential Pulse-Shape Selection Methods," *Nucl. Instrum. Methods* **100**, 285 (1972).
49. Z. H. Cho and J. Llacer, "Timing with High Purity Germanium Coaxial Detector," *Nucl. Instrum. Methods* **98**, 461 (1972).
50. F. Gabriel, H. Koepernik, and K. Schops, "A Timing System for Ge(Li) Detectors," *Nucl. Instrum. Methods* **103**, 501 (1972).
51. C. Bohm and Z. H. Cho, "A Computer Study of Time Resolutions and Charge Collection Times of Ge Gamma-Ray Detectors with Currently Employed Time Pick-Off Techniques," *IEEE Trans. Nucl. Sci.* **NS-20**, 246 (1973).
52. L. Karlsson, "On a Timing Circuit for Ge(Li) Detectors," *Nucl. Instrum. Methods* **106**, 161 (1973).
53. W. J. McDonald and D. C. S. White, "Triple Constant-Fraction Discriminator," *Nucl. Instrum. Methods* **119**, 527 (1974).
54. P. G. Coulter, H. C. Evans, and B. C. Robertson, "The Dependence of Ge(Li) Timing Information on Gamma-Ray Intensity Distributions," *Nucl. Instrum. Methods* **117**, 239 (1974).
55. M. R. Maier and D. A. Landis, "Second Version of a Constant-Fraction Trigger Redesigned with New Integrated Circuits and Results with Semiconductor Detectors," *Nucl. Instrum. Methods* **117**, 245 (1974).
56. M. Y. El-Ibiary and L. A. El-Kharadly, "Analytical Study of Amplitude Risetime Compensated Timing with Germanium Planar Detectors," *IEEE Trans. Nucl. Sci.* **NS-21**, 23 (1974).
57. D. C. S. White and W. J. McDonald, "Recent Developments in Subnanosecond Timing with Coaxial Ge(Li) Detectors," *Nucl. Instrum. Methods* **115**, 1 (1974).
58. T. Lakatos and G. Mathe, "Accurate Amplitude Measurement and Time Pick-Off Method for the Broad Pulse Width Range of Nuclear Detectors," *Nucl. Instrum. Methods* **123**, 579 (1975).
59. J. Kozyczkowski and J. Bialkowski, "Amplitude and Rise Time Compensated Timing Optimized for Large Semiconductor Detectors," *Nucl. Instrum. Methods* **137**, 75 (1976).

60. M. Bedwell and T. J. Paulus, “A New Constant Fraction Timing System with Improved Time Derivation Characteristics,” *IEEE Trans. Nucl. Sci.* **NS-23**(1), 234 (1976).
61. M. Y. El-Ibiary and L. A. El-Kharadly, “A Generalized Analysis of Zero Cross Over Timing Systems for Semiconductor Detectors,” *IEEE Trans. Nucl. Sci.* **NS-23**, 1275 (1976).
62. M. O. Bedwell, “The Application of a Rejection Technique for Slow Risetime Signals to ARC Timing with a Ge(Li) Detector,” Ph.D. dissertation, The University of Tennessee, Knoxville (1976).
63. L. L. Gadeken and B. C. Robertson, “The Influence of Ge(Li) Detector Pulse Shape Variations on Constant-Fraction and Snap-Off Timing Discriminators,” *Nucl. Instrum. Methods* **136**, 255–259 (1976).
64. T. Raudorf, T. J. Paulus, M. Bedwell, and M. Martini, “Comparative Timing Performance of Large-Volume Ge(Li) and HPGe Coaxial Detectors,” *IEEE Trans. Nucl Sci.* **NS-24**(1) 78 (1977).
65. H. Engel, H. Schneider, and R. Spitz, “A Pulse Shape Selection Method to Improve the Timing Properties of a Large Ge(Li) Detector,” *Nucl. Instrum. Methods* **142**, 525–530 (1977).
66. B. C. Robertson and H. L. Malm, “Timing Properties of Coaxial HPGe Detectors,” *Nucl. Instrum. Methods* **150**, 401 (1978).
67. B.C. Robertson, “An Evaluation fo the Triple Constant Fraction Discriminator,” *Nucl. Instrum. Methods* **152**, 575–576 (1978).
68. M. Y. El-Ibiary, “Event Timing in High Purity Germanium Coaxial Detectors,” *IEEE Trans. Nucl. Sci.* **NS-27**(2), 984–988 (1980).
69. T. W. Raudorf, T. J. Paulus, and R. C. Trammell, “Characterization of a Large HPGe Coaxial Detector,” *Nucl. Instrum. Methods* **176**, 595 (1980)
70. M. Y. El-Ibiary, “Zero Cross-Over Timing with Coaxial Ge(Li) Detectors,” *IEEE Trans. Nucl. Sci.* **NS-27**(2), 974–983 (1980).
71. B. C. Robertson, “The Influence of Charge Collection Characteristics on HPGe Detector Timing Performance,” *Nucl. Instrum. Methods* **169**, 465–468 (1980).
72. K. W. Renner, M. O. Bedwell, and J. F. Pierce, “A Wideband Direct Coupled Amplifier Utilizing a Fast/Slow Loop Concept,” *IEEE Trans. Nucl. Sci.* **NS-28**(1), 584 (1981).
73. T. J. Paulus, T. W. Raudorf, B. Coyne, and R. C. Trammell, “Comparative Timing Performance of Large Volume HPGe Detectors,” *IEEE Trans. Nucl. Sci.* **NS-28**(1), 544–548 (1981).

Silicon Surface-Barrier Detector Timing

74. I. S. Sherman, R. G. Roddick, and A. J. Metz, “A Low Walk, High Resolution Timing System for Silicon Detectors,” *IEEE Trans. Nucl. Sci.* **NS-15**(3), 500 (1986).
75. E. E. Gross, “A Theoretical Comparison of Two Methods for Timing with Surface Barrier Detectors.” Ph.D. dissertaton, The University of Tennessee, Knoxville (1972).
76. T. J. Paulus, R. D. McKnight, and T. L. Mayhugh, “Experimental Characterization of the Timing Properties of a Detector-Preamplifier System for Charged Particle Detectors Using a Laser Pulser,” *IEEE Trans. Nucl. Sci.* **NS-24**(1), 335 (1977).
77. N. Karlovac and T. L. Mayhugh, “A Fast Low-Noise Charge Preamplifier,” *IEEE Trans. Nucl. Sci.* **NS-24**(1), 327 (1977).

Photon Counting and Photomultiplier Tubes

78. L. G. Hyman, R. M. Schwarcz, and R. A. Schluter, “Study of High Speed Photomultiplier Systems,” *Rev. Sci. Instrum.* **35**(3), 393–406 (1964).
79. C. R. Kerns, “Photomultiplier Single-Electron Time-Spread Measurements,” *IEEE Trans. Nucl. Sci.* **NS-14**(1), 449–454 (1967).
80. A. T. Young, “Photometric Error Analysis. IX: Optimum Use of Photomultipliers,” *Appl. Opt.* **8**(12), 2431–2447 (1969).
81. R. Foord, R. Jones, C. J. Oliver, and E. R. Pike, “The Use of Photomultiplier Tubes for Photon Counting,” *Appl. Opt.* **8**(10), 1975–1989 (1969).
82. P. B. Coates, “Noise Sources in the C31000D Photomultiplier,” *J. Phys. E: Sci. Instrum.* **4**, 201–207 (1971).
83. ORTEC, “The Single-Photon Technique for Measuring Light Intensity and Decay Characteristics,” *Application Note 35*, Oak Ridge, Tennessee (1971).
84. S. Cova, M. Bertolaccini, and C. Bussolati, “Single Photon Techniques for Precision Measurements of Optical Waveforms from Radiative Decays,” *IEEE Trans. Nucl. Sci.* **NS-19**(3), (1972).
85. J. D. Ingle, Jr. and S. R. Crouch, “Critical Comparison of Photon Counting and Direct Current Measurement Techniques for Quantitative Spectrometric Methods,” *Anal. Chem.* **44**(4), 785–794 (1972).
86. “IEEE Standard Test Procedures for Photomultipliers for Scintillation Counting and Glossary for Scintillation Counting Field, *IEEE* (1972).
87. F. de la Barre, “Influence of Transit Time Differences on Photomultiplier Time Resolution,” *Nucl. Instrum. Methods* **102**, 77–86 (1972).
88. R. Reisse, R. Creecy, and S. K. Poultney, “Single Photon Detection and Sub-Nanosecond Timing Resolution with the RCA C31034 Photomultiplier,” *Rev. Sci. Instrum.* **44**(11), 1666–1668 (1973).
89. D. V. Kerns, Jr., T. M. Chen, and S. T. Hsu, “The Influence of Biasing Circuits on Photomultiplier Tube Output Noise Spectra and Transfer Functions,” *IEEE Trans. Electron Devices* **ED-20**(4), 311–317 (1973).

90. B. Sipp and J. A. Miehe, “Influence of the Time-of-Flight Spread of Photoelectrons on the Measurements of the shape of Subnanosecond Light Pulses in 8850 RCA Photomultipliers,” *Nucl. Instrum. Methods* **114**, 249–253 (1974).
91. C. C. Lo and B. Leskovar, “A Measuring System for Studying the Time-Resolution Capabilities of Fast Photomultipliers,” *IEEE Trans. Nucl. Sci.* **NS-21**(1), 93 (1974).
92. W. Fichtner and W. Hacker, “Time Resolution of Ge Avalanche Photodiodes Operating as Photon Counters in Delayed Coincidence,” *Rev. Sci. Instrum.* **47**(3), 374–377 (1976).
93. L. J. Cline Love and L. A. Shaver, “Time Correlated Single Photon Technique: Fluorescence Lifetime Measurements,” *Anal. Chem.* **48**(4), 364–371 (1976).
94. P. R. Hartig, K. Sauer, C. C. Lo, and B. Leskovar, “Measurement of Very Short Fluorescence Lifetimes by Single Photon Counting,” *Rev. Sci. Instrum.* (1976).
95. B. Leskovar, C. C. Lo, P. R. Hartig, and K. Sauer, “Photon Counting System for Subnanosecond Fluorescence Lifetime Measurements,” *Rev. Sci. Instrum.* **47**, 9 (1976).
96. M. Moszynski and J. Vacher, “Influence of Incident Light Wavelength on Time Jitter of Fast Photomultipliers,” *Nucl. Instrum. Methods* **141**, 319–323 (1977).
97. R. D. Hiebert, H. A. Thiessen, and A. W. Obst, “Photomultiplier Tube Base for High Pulsed Anode Currents,” *Nucl. Instrum. Methods* **142**, 467–469 (1977).
98. C. R. Kerns, “A High-Rate Phototube Base,” *IEEE Trans. Nucl. Sci.* **NS-24**(1), 353–355 (1977).
99. G. Spears, E. Cramer, and L. Hoffland, “Subnanosecond Time-Correlated Photon Counting with Tunable Lasers,” *Rev. Sci. Instrum.* **49**(2), 255–262 (1978).
100. F. Calligaris, P. Ciuti, I. Gabrielli, and R. Giacomich, “Theoretical Model of Light-Pulse Propagation in Pipes Verified by Single-Photon Technique,” *Nucl. Instrum. Methods* **148**, 323–330 (1978).
101. V. J. Koester and R. M. Dowben, “Subnanosecond Single Photon Counting Fluorescence Spectroscopy Using Synchronously Pumped Tunable Dye Laser Excitation,” *Rev. Sci. Instrum.* **49**(8), 1186–1191 (1978).
102. G. R. Haugen, B. W. Wallin, and F. E. Lytle, “Optimization of Data-Acquistion Rates in Time-Correlated Single-Photon Fluorimetry,” *Rev. Sci. Instrum.* **50**(1), 64–72 (1979).
103. K. A. Z. A. Hussain and D. K. Butt, “Time Resolution Studies of Fast Photomultipliers,” *Nucl. Instrum. Methods* **173**, 471–475 (1980).
104. S. Kinoshita, H. Ohta, and T. Kushida, “Subnanosecond Fluorescence-Lifetime Measuring System Using Single Photon Counting Method with Mode-Locked Laser Excitation,” *Rev. Sci. Instrum.* **52**(4), 572–575 (1981).
105. M. A. Raoof and S. A. Raoof, “Timing Coincidence Studies with Fast Photomultipliers,” *Nucl. Instrum. Methods* **185**, 215–218 (1981).

General

106. W. J. Price, Nuclear Radiation Detection, McGraw-Hill Book Co., New York, NY (1964).
107. P. W. Nicholson, Nuclear Electronics, John Wiley and Sons, Inc., New York, NY (1974).
108. J. Gal, “Investigation of the Jitter of the Constant Fraction Timing Method Based on the Comparison of the Original Signal and the Stretched and Attenuated One,” *Nucl. Instrum. Methods* **133**, 341 (1976).
109. J. E. Draper, “The Effect of the Randomizing Time on the Shape of a Timing Distribution,” *Nucl. Instrum. Methods* **151**, 267–270 (1978).
110. *Poistron Annihilation*, Proc. 5th Int. Conf. Positron Annihilation, Japan (1979).
111. G. F. Knoll, *Radiation Detection and Measurement*, John Wiley and Sons, New York, NY (1979).

AN42
Application Note

Specifications subject to change
122908

ORTEC®

www.ortec-online.com

Tel. (865) 482-4411 • Fax (865) 483-0396 • ortec.info@ametek.com
801 South Illinois Ave., Oak Ridge, TN 37831-0895 U.S.A.
For International Office Locations, Visit Our Website

AMETEK®
ADVANCED MEASUREMENT
TECHNOLOGY